

**EVALUATION OF COMPUTED TOMOGRAPHY
TO DETERMINE THE DISTRIBUTION OF
MACROPORES IN SOIL**

By

Glenn S. Warner

and

John L. Nieber

Department of Agricultural Engineering
University of Minnesota
St. Paul, MN 55108

Technical Report Number 133
Water Resources Research Center
University of Minnesota
St. Paul, MN 55108

June 1991

This project serves as the final completion report for the Water Resources Research Center Project directed by John L. Nieber of the Department of Agricultural Engineering, University of Minnesota. It is Number 133 in the Technical Completion Report series.

The work upon which this publication is based was supported in part by funds provided by the U.S. Department of the Interior, U.S. Geological Survey, and the Water Resources Research Center, University of Minnesota, as authorized by the Water Resources Research and Development Act of 1984.

Contents of this publication do not necessarily reflect the views and policies of the U.S. Department of the Interior, nor does mention of trade names of commercial products constitute their endorsement by the U.S. Government.

The University of Minnesota is an equal opportunity employer and educator.

Water Resources Research Center
Graduate School
University of Minnesota
Room 302, 1518 Cleveland Ave. N.
St. Paul, MN 55108

CONTENTS

	Page
Abstract	1
1. Introduction	3
1.1. Background	3
1.2. Preferential Flow in Soil	3
1.3. Impacts of Macropores in Hydrology	4
1.4. Characterization of Macropores	6
1.5. Objective	7
2. Application of CT to Soil	8
2.1. Introduction to CT	8
2.2. Previous Applications of CT to Soil Materials	11
2.3. Discussion	16
3. Study Methodology	18
3.1. Specific Objectives	18
3.2. Field Cores	18
3.3. Packed Cores as Standards	20
3.4. CT Scanner Parameters	20
3.5. Image Display and Analysis	23
3.6. Sectioning of Cores	23
3.7. Analysis of Data from Silt and Sand Standards	24
3.8. Quantitative Characterization of Macropores	24
4. Results	27
4.1. Qualitative Results of Field Cores: Photos of CT Images and Physical Sections	27
4.2. Results of Sand and Silt Standards Analyses	32
4.3. Quantitative Results for Field Cores	39
5. Discussion, Recommendations and Conclusions	45
5.1. Visual Identification of Macropores Using CT Images	45
5.2. Use of Microcomputers for CT Image Display and Analysis	45
5.3. Analyses of Results from Sand and Silt Standards	47
5.4. Analyses of Field Cores	48
5.5. Recommendations	49
5.6. Scanner Selection and Future Development	50
5.7. Image Analysis	50
5.8. Future Work	51
Conclusions	51
References	52

EVALUATION OF COMPUTED TOMOGRAPHY TO DETERMINE THE DISTRIBUTION OF MACROPORES IN SOIL

Abstract

Preferential flow paths in some soils result in the rapid movement of water and associated chemicals to groundwater. Macropores are one type of preferential path. Examples of macropores include earthworm tunnels, decayed root channels, shrink/swell cracks, tillage cracks, etc. Water movement through a soil can potentially be modeled if the number, size and extent of the macropores are known. At present no easy and accurate method of characterizing macropores has been developed. X-ray computed tomography (CT), developed for medical purposes, uses scan techniques to secure multiple views of an object and provides a means of obtaining nondestructive internal cross sections of objects. The spatial resolution of modern scanners is on the order of 1 mm, providing a potential means of detecting small air-filled pores within the soil.

Undisturbed soil cores, 200 mm in diameter, were taken in cultivated and uncultivated areas. A medical CT scanner was used to scan these cores at depth intervals varying from 10 mm to 50 mm. Data for each scan were analyzed using microcomputers to display images and to determine the size and number of macropores for each scan image. Cores were physically sectioned at scan locations to visually compare the size, location and continuity of macropores in the sections with those shown in the scan images.

Laboratory cores packed with soil were scanned as standards to determine the response and contrast resolution of the CT scanner for dense material containing sharp density discontinuities. Cores were packed with different types and densities of soil. Artificial "macropores" were formed in some packed cores using glass tubes and holes formed with wire probes to assess the resolution of the scanner.

Macropores of various sizes and types were found in all of the field cores scanned with the majority of macropores being associated with earthworm tunnels. The number and size of macropores were approximately the same for all cores below a depth of approximately 50 mm. The number of macropores found above this depth was affected by a large number of roots in the grass-surfaced core and by tillage in the bare-surfaced core. Many macropores were continuous to depths of 600 mm or more. Some passed completely through the core. Dye tests and physical sampling revealed that some of the macropores functioned as preferential flow paths and had very high flow rates.

Analysis of the packed cores revealed that the detection of small holes in a dense medium by CT depends not only on the size of hole but also on the density of the medium. Various attenuation values were examined to determine the optimal threshold value to use for the detection and measurement of macropores in the field cores. The average attenuation value for air in the holes in the cores was not zero as was initially assumed, but varied with the size of hole.

The results showed that a CT scanner can accurately determine pore locations and sizes for pores 1 mm or larger. Accurate determinations of macropore characteristics require that proper values of parameters for the medium and conditions being analyzed be assessed. Use of microcomputers greatly enhanced the ability to display images, analyze features of interest, detect and characterize individual macropores. The main conclusion of the study was that the CT scanner when coupled with use of computers is a potentially valuable tool for characterizing macropores.

1. INTRODUCTION

1.1 Background.

The movement of water into (infiltration) and through (percolation) soil are critical components of the hydrologic cycle. Infiltration is the determining factor for the amount and rate of surface runoff for a given precipitation event, while percolation affects the amount of water available for plant growth, the travel time of water through the soil profile, recharge of groundwater and subsurface flow to streams. Until the late 1970's, the primary emphasis in the study of these processes dealt with water quantity, e.g. amount of surface runoff and soil water recharge. However, infiltration and percolation have major water quality impacts such as the movement of dissolved chemicals (solutes) or suspended matter through the soil and into groundwater.

The importance of groundwater quality is manifested by the large use of groundwater for domestic water supply. Nationwide, approximately 50 percent of the population obtains its drinking water from groundwater sources, while more than 80 percent in rural areas rely on groundwater (Office of Technology Assessment, 1984). During the past decade, major concerns have been raised about the quality of these water supplies due to chemicals commonly used in intensive agriculture. Chemicals found in fertilizers and pesticides used in agriculture have been detected in both shallow and deep groundwater aquifers. A Minnesota survey from July, 1985 to June, 1987 revealed that one or more pesticides were found in 39% of 500 wells tested (Klaseus et al., 1988). A 1988 nationwide survey revealed that one or more of 67 different pesticides were detected in 33 of 35 states responding (Parsons and Witt, 1988).

Widespread occurrence of agricultural pesticides has also been found in surface waters. The U.S. Geological Survey (USGS) found detectable amounts of triazine herbicides in 55% of 150 streams sampled in 10 midwestern states in early spring of 1989 before new applications of herbicides to fields. Sampling in May and June, after herbicides had been freshly applied to most fields, showed detectable levels in about 90% of streams sampled. Samples collected in May and June revealed that 44 out of 127 sites had levels of alachlor exceeding the proposed U.S. Environmental Protection Agency's proposed maximum level in drinking water, while 71 sites exceeded the recommended level for atrazine, 15 exceeded the level for cyanazine and 5 exceeded the level for simazine (U.S.G.S., 1989). It is this relative recent recognition of potential impacts on both surface and groundwater quality that has motivated researchers to better understand water movement in soils.

1.2 Preferential Flow in Soil.

During the last 50 years, the many studies of water movement in soil (or other porous media) have usually assumed that the soil can be represented as a homogeneous medium and assumed that vertical movement of soil water was uniform across a horizontal plane. A large number of models have been developed which use these assumptions for prediction of infiltration and resulting runoff or for groundwater recharge. However, during the 1980's a number of researchers have observed phenomena both in the laboratory and the field which cannot be explained by use of such models. Recent research has attempted to explain some of the phenomena, including the finding of pesticides in deep groundwater supplies, by the presence of **preferential flow paths** in the soil or medium. Preferential flow paths result in non-uniform movement of water through the soil and consequently more rapid transit of water and constituents to groundwater aquifers.

The term *preferential flow* refers to that flow that follows selected paths through a porous medium rather than flowing uniformly through the entire cross sectional matrix of the medium. Preferential flow is contrasted with uniform flow where water moves as an even front through the medium. Fig. 1.1 shows illustrations of uniform and preferential flow for the downward movement of water in soil.

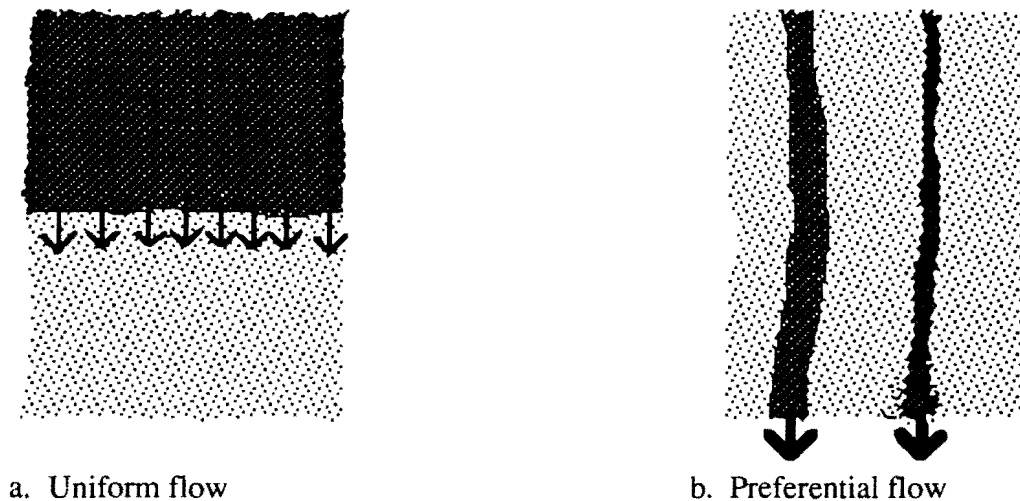


Figure 1.1 Illustrations of Uniform and Preferential Flow.

Several types of preferential flow paths may occur in soil. These types may result from heterogeneous or anisotropic conditions in the soil or from instabilities due to fluid(s)-medium interactions. One categorization of preferential flow is : 1) Wetting Front Instabilities, 2) Soil Heterogeneities, and 3) Macropores. Further explanations and references for the categories can be found in Warner (1990). Macropores, from the word *macro* meaning large, is used to mean a pore significantly larger than the intergranular or inter-aggregate pores within the general soil matrix. In addition to the difference in relative size when compared to intergranular or inter-aggregate pores, a macropore can be thought of as being different in formation and continuity.

Macropores may be produced by either physical or biological processes. Examples of physical processes include the shrink/swell phenomena caused by the drying and wetting of certain soils, hydraulic pressures causing subsurface erosion, freezing and thawing, and man-induced processes such as tillage. Biological processes include actions by earthworms, insects and other animals and those caused by plant roots. Beven and Germann (1982) provide a thorough overview of the different types of macropores. In all these examples the macropore is formed by external forces or actions that are independent of the inherent structural formation of the soil and which are temporal in nature. The pores formed by these forces are not entirely random and are at least semi-isotropic, i.e. they are roughly continuous in size and shape along one axis at least for several centimeters or more. In an attempt to standardize the term, *macropore*, Luxmoore (1980) suggested be those pores larger than 1 mm in diameter based on a functional relationship between capillary pressure and size of pore. Other researchers have argued for other size or functional definitions. A detailed discussion of the subject may be found in Warner (1990).

1.3 Impacts of Macropores in Hydrology.

Water penetration into a homogeneous soil system without macropores is assumed to occur through the small pores or voids among the grains or aggregates. This type of flow is often referred to as *matrix* flow since the flow of water is through the matrix of small pores. Another term used to describe this type of flow is *piston* flow since a wetting front for homogeneous conditions will move uniformly through the profile as a piston does within a cylinder. The flow capacity of the soil for matrix flow is governed by the size and connectivity of the intergranular or inter-aggregate soil voids. Usually the flow is considered to follow Darcy's law. However, where macropores exist, water flow in the soil may be dominated by movement through the macropore system, especially for near-saturated conditions. Flow through macropores is much faster than through the soil matrix system and is usually non-Darcian (Edwards et al., 1979; Germann and Beven, 1985).

Soil macropores were known to exist as long ago as the nineteenth century as indicated by

Thomas and Phillips (1979) and Beven and Germann (1982), but only recently has much emphasis been placed on their importance in hydrologic processes. Macropores can greatly affect a number of interrelated processes. For example, the presence of macropores in soils has been shown to greatly influence the infiltration rate and movement of water within a soil profile (Edwards et al., 1979; Germann and Beven, 1981; Germann and Beven, 1985; and Lee, 1985). For a given rainfall, the infiltration rate inherently determines the excess rainfall, i.e. the surface runoff rate. The runoff in turn affects the discharge to stream channels and the erosion potential. Other processes potentially affected by macropores include: soil water distribution, aeration of soil, drainage efficiency (Steenhuis, et al., 1986), groundwater recharge, salt accumulation and movement, root penetration and crop yield, irrigation efficiency and water loss.

In hydrology the presence of preferential flow in soil or geologic formations can greatly impact the rate at which surface water reaches groundwater systems. If water flows at a uniform rate through soil the travel time to underlying aquifers will be much longer than if the water flows in preferential flow paths at the same overall flux or discharge but through a much smaller cross sectional area. Consequently, any solutes in the water will be delivered to the groundwater much quicker than for the uniform flow assumption. This consequence has major implications for groundwater quality, especially when surface applied chemicals commonly used in present-day agriculture are considered. Under the uniform flow theory, many chemicals are assumed to be adsorbed to soil particles as the solutes slowly pass through the very small pores among soil particles. The path length among the particles is assumed to be long so there is thought to be ample opportunity for the solutes to attach to particles. If the flux is following a preferential flow path, there may not be sufficient surface area of soil particles along the path to adsorb and tie up any solutes that are usually attracted to soil surfaces.

For solutes which are not readily adsorbed to particles, the assumption is often made that the slow travel rate allows time for plants to absorb the solutes (such as nitrogen) during their growing process. In addition the slow rates allow time for breakdown of chemicals such as pesticides into compounds that are considered to be less harmful. The breakdown process is a function of temperature, oxygen content, organic matter content and microbial action, all of which are almost always higher in the upper soil layers during the growing season. At deeper soil layers or geologic formations there is much less microbial action that can rapidly break down or use pesticides or nutrients. Once these solutes pass through the biologically active upper soil layers, there is little opportunity for uptake or breakdown of the solutes and they will be carried to the groundwater by the downward water flux.

Many hillslope processes may also be a function of the number, size and orientation of macropores present along a slope. The presence of macropores, particularly if oriented along the slope as well as vertically, will govern the amount of shallow subsurface discharge or interflow. For instance, in recent field and computer studies, Steenhuis et al. (1986) and Richard and Steenhuis (1987) demonstrated that movement of surface water and solutes to drainage tile lines was more than two orders of magnitude faster than would be predicted by Darcian flow through the soil matrix. The subsurface discharge along with topography will determine the extent and location of saturated source areas, timing and amount of discharge to surface channels, erosion, slope stability, and other hydrologic characteristics. In most forested landscapes, surface runoff is rare but yet substantial discharges in streams occur relatively rapidly following even moderate rainfalls. A number of investigators have shown that the rapid response is due to shallow subsurface flows occurring in macropores or soil pipes (Whipkey, 1967; Mosley, 1979 and 1982, Hewitt and Hibbert, 1967; Harr, 1977; and Steenhuis, et al., 1986).

The presence of macropores may also affect microbial movement in the soil. Germann et al. (1987) applied a kinematic wave model to the movement of *Escherichia coli* through a soil with macropores. They obtained threshold values of water content and conductance within the macropores for substantial movement of microbes into the groundwater system. Rahe et al. (1978) measured the movement of *E. coli* under saturated flow conditions on a hillside. They found rates of movement much higher than could be explained by uniform flow theory and attributed the high rates to rapid movement in macropores.

From the studies mentioned above, it is apparent that macropores can greatly affect

hydrologic processes and may play an important role in the movement of pollutants to groundwater. However, the impact of macropores on contamination of groundwater is more complicated than first seems. The impacts could possibly be either beneficial or detrimental depending on specific circumstances. If a potential contaminant is well mixed within a soil, the presence of macropores could actually reduce the potential for the contaminant to reach the groundwater by providing a pathway which bypasses the soil matrix. Rainfall that entered macropores near the soil surface would not leach or mix with the matrix soil water and should be relatively clean. The experiment by Wild and Babiker (1976) where the solutes were applied to the soil surface and allowed to uniformly enter the soil before application of large amounts of water is an example of bypass of matrix solutes due to macropores. In that experiment, the maximum depth to which some solutes were carried was greater, but the center of mass of solutes was closer to the surface where macropores were present compared to where they were not.

However, if a contaminant is contained in applied water or is not well mixed within the soil, macropores may provide a pathway for rapid movement of the water and contaminant. Application of fertilizers or pesticides through irrigation water to certain soils may be an example where potential pollutants could be rapidly transmitted to groundwater if macropores are present. Material on the surface may also be dissolved or suspended by surface waters before entering macropores. In addition if water dissolves solutes after passing through upper portions of the soil profile and then enters macropores, the overall effect may also be detrimental. Also, although macropores may bypass the major part of solutes mixed within the soil matrix as indicated above, the amount carried deeper and faster to groundwater may prove critical.

The above studies illustrate that it is difficult to assign a general, overall impact to macropores and that the impacts of macropores must be addressed for specific circumstances. This requires that the size, type, number and extent of macropores be determined for a site. Also the flow characteristics of macropores at different depths, entrance conditions, soil moistures and rates of applied water must be known. Once the physical dimensions and flow characteristics are known, different conditions can be modeled mathematically to assess impacts of macropores for a given situation. The studies do show that the existence and influences of macropores should not be ignored when attempting to understand hydrologic processes within soil.

1.4 Characterization of Macropores.

To assess the impact of macropores on the flow and transport properties of soils, the size, number, type, distribution and continuity of macropores in the soils must be characterized. This characterization can be accomplished by two approaches. The first approach is to measure water and solute concentration fluxes through representative soil cores either in the field or laboratory. Some of the physical attributes of the pore structure within the cores can then be derived by application of known physical laws to the observed fluxes. This is an indirect approach since the shape, size, number and extent of preferential flow paths are not fully known, but only their influence under specific experimental conditions. The second, direct approach, involves determining the physical dimensions of the macropores by measuring the shape, size, number and extent of macropores.

Indirect approaches include such methods as 1) Hydraulic conductivity measurements of soil cores in the laboratory or infiltration measurements in the field using both positive and negative soil-water pressures (Watson and Luxmoore, 1986; Moore et al., 1986), and 2) Solute-concentration breakthrough curves from soil cores. Anderson and Bouma (1977), Bouma and Wosten (1979), Gish and Jury (1982) and others have used chloride breakthrough curves from undisturbed soil columns as an indirect means of characterizing macropores. These indirect methods can only describe the function of macropores for the initial and boundary conditions for the given experiments. The physical characterization is still largely unknown as is their function or response for different conditions. For this reason a more direct approach of characterization is preferable although perhaps more difficult.

Direct approaches include: 1) use of adsorbed dyes to mark macropores (Ehlers, 1975; Smettem and Collis-George, 1985b; Omoti and Wild, 1979; and Richard et al., 1988), 2) filling of selected macropores with hardeners (Green and Askew, 1965; Smettem and Collis-George,

1985a), 3) image analysis of impregnated sections of soil (Jongerius et al., 1972; Bouma et al., 1977; Bullock and Thomasson, 1979; Beven and Germann, 1982; Ringrose-Voase and Bullock, 1984; and Pikul et al., 1988), 4) field measurement using photographs (Edwards et al., 1988), and 5) scanning techniques using computed tomography.

Summaries of the referenced studies for the first four direct approaches can be found in Warner (1990). These four direct methods have the disadvantage of being destructive type methods, i. e. to determine the macropores the soil mass must be physically sectioned or removed. This limits their application as they cannot be repeatedly applied to study changes in macropores over time for different conditions such as earthworm populations, root growth, water contents, etc. Scanning methods involve measurement of internal properties of soil samples using energy sources which although invasive are nondestructive and nonperturbing. The attenuation of the energy as it passes along a narrow path (one view) through the object is measured. The distribution of properties within the object can then be calculated by making multiple view measurements. Scanning has the disadvantage of requiring removal of samples from the field for analysis.

1.5 Objective.

The objective of the present study was to evaluate the use of x-ray computed tomography (CT), also known as computer aided tomography (CAT), to directly and nondestructively characterize macropore structure in soil columns. The CT scanner was developed for medical purposes but has proven useful in the field of soil science for determination of soil water content and bulk density. The following section addresses some of the theoretical aspects of CT application to soils and gives some results of previous studies (Petrovic et al., 1982; Hainsworth and Aylmore, 1983; Crestana et al., 1985; Hainsworth and Aylmore, 1986; Anderson et al. 1988; and Tollner et al., 1987).

2. APPLICATION OF CT TO SOIL

2.1 Introduction to CT.

The first practical CT scanner was developed in 1969 by Hounsfield (1972) for use in the medical profession where there was a great need for nondestructive, internal cross-sectional views of the human body. The word *tomography* comes from two Greek words: *tomo*, meaning slice or section and *graphy*, meaning to write or display, thus meaning to write a cross section or show a slice of an object. Technically speaking, *CT scanning* could be used to mean any scanning operation or technique irrespective of the energy or invasive source, such as gamma rays, ultrasound, x-rays, or even light. However, the term is generally used within the medical field to apply strictly to the scanning technique using x-rays and is used in that particular meaning within this report unless otherwise stated.

2.1.1 CT Scanner Principles. The CT scanner is based on the principle of constructing an image by taking multiple views using x-rays projected within a narrow plane. Detectors located on the opposite side of the object read the intensity of x-rays exiting the object. The multiple views form sets of data from which the attenuation coefficients at interior points within the object can be calculated. These attenuation coefficients are then used to construct a cross-sectional image of the plane for viewing the internal structure of the object. The image is composed of numerous small, square picture elements (pixels), each of which corresponds to a position in the object being scanned. Pixels smaller than 1.0 mm by 1.0 mm are possible on some scanners (Morgan, 1983). This resolution and its nondestructive nature make the CT scanner a valuable tool, not only in the field of medicine, but also potentially in fields such as soil science and engineering. Figure 2.1 illustrates a typical modern scanner consisting of the gantry with an x-ray tube and bank of detectors plus the patient table that can be moved incrementally through the gantry. Further explanations of CT scanner principles, basic interaction of x-rays with matter and the attenuation of x-rays through a series of materials are given by Warner (1990).

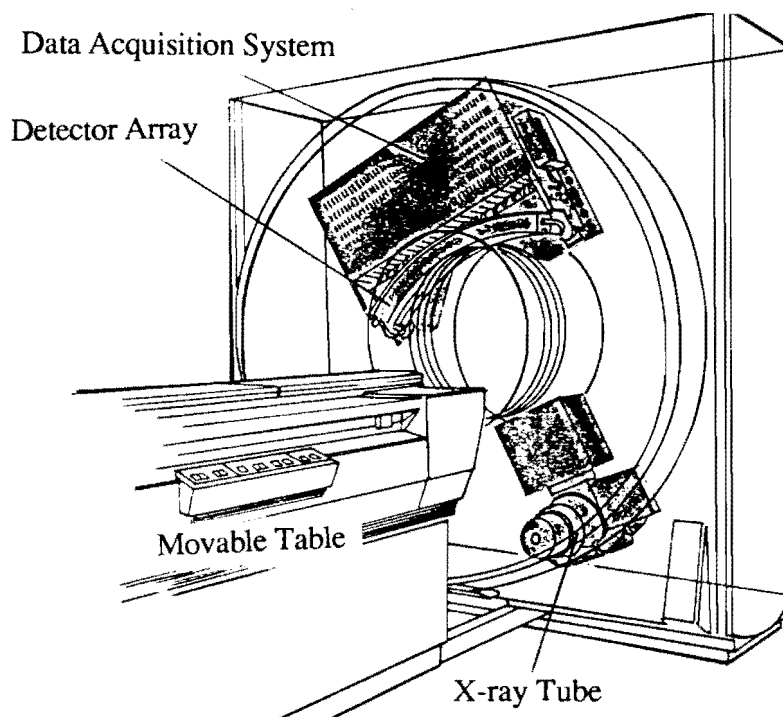


Figure 2.1 Illustration of Typical Modern Scanner.
(Adapted from General Electric CT Operating Manual.)

The linear attenuation values for individual pixels are generally converted to Hounsfield units, H , by the following equation:

$$H = \frac{\mu - \mu_{\text{water}}}{\mu_{\text{water}}} \times 1000 \quad (2.1)$$

Although μ_{water} varies with the voltage used, a commonly used value is 0.191 cm^{-1} (McCullough, 1975). Some of the first scanners used a multiplier of 500 instead of 1000 in Equation 2.1, so care must be taken in interpreting values of H published in the literature. Once H is determined and stored (rounded to nearest integer) in a computer file, an image is determined and displayed on a monitor, i.e. CRT, by assigning ranges of values of H to certain gray scales. Conventional display mode is for low values to be assigned to the black end and high values to the white end of the gray scale. Colors can also be used in the display.

2.1.2 Resolution of CT Scanners. The resolution of CT scanners may refer to either the smallest spatial dimensions, i.e. pixel size, or to the smallest changes in attenuation properties that can be detected using a scanner. The smallest pixel that can be detected is governed by geometric and reconstruction factors (Morgan, 1983). The attenuation resolution is somewhat dependent on the rate of change of the attenuation properties or contrast of the material being scanned. The greater the contrast of properties of two materials, the greater the ability to detect the presence of a small object within another object. However, the less ability there is to determine the true attenuation value of the smaller object. In other words, greater contrasts in the density of materials produces the ability to qualitatively detect a small object within a large object, but reduces the ability to accurately determine quantitatively the true value for the small object. The smaller the object the less accurate the detection both quantitatively and qualitatively.

When heterogeneous materials with sharp differentiated boundaries are scanned, there are complications in attempting to determine an attenuation coefficient. If a sharp density boundary falls in the middle of a pixel in a CT scan image rather than on the edge of the pixel, the attenuation value "seen" and calculated by the scanner is a composite or average of the values for the different materials lying within the pixel edges. This effect is known as the boundary effect and makes determination of the true attenuation value for a material more difficult. An example of the boundary effect is shown in Figure 2.2 where a circular object is overlaid on a square pixel grid. In this example the large mass is assumed to have an attenuation value of 1000 while the material within the circle has a value of 0. The values shown for the pixels where the perimeter of the circle falls are theoretical values based on the proportion of the pixel covered by the dense material.

The boundary effect is especially critical when trying to detect a small object embedded within a much larger mass. If the object is smaller than or approximately the same size as the pixel, it may not be detected as the object may not fully occupy a single pixel. The scanner would not discern the true attenuation value for the object and therefore not differentiate the object from the surrounding material. Theoretically, if an object is twice as big as the pixel size, at least one pixel should fall entirely upon the object only, and therefore produce the true attenuation value for the material in the object. As an object gets larger with respect to the pixel size the overall boundary effect on the average attenuation value for the object becomes less. If the true shape of the object being scanned is known, e.g. a circle, some of the boundary effects can be corrected using edge enhancement techniques upon analysis of the scan data. If corrective measures can not be used, the only way to reduce the boundary effects is to use as small a pixel size as possible.

The partial volume effect is similar to the boundary effect for three dimensions. Whereas the boundary effect is the result of the physical relationship of an object to the location of the pixels in the x , y or cross sectional plane, the partial volume effect results from variation of the object along the z or longitudinal plane perpendicular to the rotation plane of the x-ray source and detectors. The detectors in a scanner count the number of photons that pass through the object being scanned and in effect, averages them over the slice width of the x-ray source. The attenuation value produced for a pixel is therefore an average for the three dimensional pixel or voxel. For objects that are homogeneous in the z direction, the slice width used will not be of major concern.

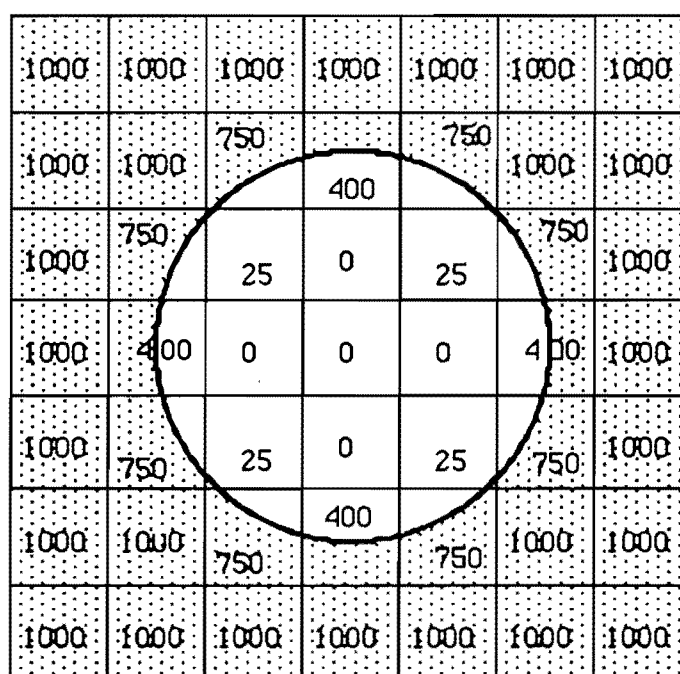


Figure 2.2 Schematic of Boundary Effects for Circular Object.

However, for objects that vary longitudinally due to varying cross sectional shape or size or whose cross sections are not orthogonal to the rotation plane, the slice width will affect the average attenuation value for the voxel. An example is a perfectly circular tube that is aligned at some angle other than 90 degrees to the scan rotation. The resultant shape of the circle as seen by the scanner will be an oval. If the slice width is very narrow the partial volume effect will be minimal, but larger slice widths will result in attenuation values and images that may be misleading.

The boundary effects will be of concern for detection of macropores within a soil sample. Macropores for the definitions and conditions studied here will be air-filled and therefore should have a significantly different attenuation coefficient than the surrounding soil matrix, making detection of macropores theoretically possible. However, the small size of macropores will produce problems since some macropores may be the same size or smaller than the pixel size of the scanner. The partial volume effect is also of concern in the use of CT to detect and characterize macropores since some macropores may not be directly vertical to the surface but may be at a diagonal or may meander. A larger slice width provides less noisy data for a uniform cross section since the attenuation of the x-ray beam is averaged over the slice width. For an isotropic material, i.e., uniform along the axis perpendicular to the scan cross section, a larger slice width will average any partial volume effects and produce a greater contrast.

2.1.3 Artifacts. There are a number of artifacts that may result from a CT scan. An artifact is an appearance in an image that does not accurately represent the object being scanned. Examples include streaks radiating from a point, denser portions of an image of a homogeneous object, and distortions of shapes of the object. Artifacts may be produced by geometric effects incorporated within the design of the machine, by alterations in the energy spectrum of the x-ray beam, by inherent deficiencies of the reconstruction algorithm, or by measurement errors. Artifacts may be considered as a source of noise according to Morgan (1983), who devotes an appendix to the subject.

One of the more troubling artifacts results from the alteration in the energy spectrum of the x-ray beam and is called *beam hardening*. This artifact results from the lower-energy photons

being preferentially absorbed as the x-ray beam passes through a dense object. As the beam progresses the average photon energy increases. Consequently, the beam is said to become harder. The attenuation is a function of photon energy, decreasing as the energy increases. Consequently, the apparent attenuation values in pixels on the perimeter of an object will be greater than for pixels of the same exact material and density in the center of the scanned object. Beam hardening is especially a problem when the perimeter is more dense than the center such as in the human head. It is also more of a problem where higher Z materials are scanned since the coherent scattering and photoelectric effects are greater and are nonlinear functions of Z . Where significant beam hardening occurs, it is difficult to compare the density distributions within a material.

Beam hardening can be reduced but not eliminated by filtering the x-ray beam as it leaves the x-ray tube. Filtering removes the low-energy portion of the spectrum, thereby partially hardening the beam before it reaches the object to be scanned. Beam hardening can be corrected for in part through modifications in the reconstruction algorithm, use of a water bath, by postreconstruction adjustments in the image data, or through dual scanning techniques (Morgan, 1983).

2.2 Previous Applications of CT to Soil Materials.

In recent years several investigators have recognized the potential of CT scanning to obtain nondestructive views of objects other than the human body. In the field of soil science, CT scanners have been investigated for the possible determination of bulk density or water content (Petrovic et al., 1982; Hainsworth and Aylmore, 1983 and 1986; Crestana et al., 1985; Brown et al., 1987; Tollner and Verma, 1987; Tollner and Ramseur, 1988; and Anderson et al., 1988). The CT scanner was developed for specific use in the medical field involving the human body. Its design and operating parameters have accordingly been optimized for soft tissue with attenuation values near that of water. Consequently, there is a need to investigate the applicability of its design and operating parameters to more dense material such as soil.

The advantages of CT include the nondestructive nature permitting repeated measurements over time or space, the continuity of the measurements allowing continuous measurements along any axis, the speed of the measurements allowing analysis of dynamic phenomena, the nonperturbing nature or non-interfering nature of the method, the sensitivity of small changes in water content, and the relative small dimensional resolution available.

In one of the first studies involving soil science, Petrovic et al. (1982) assessed the use of CT scanning for determination of soil bulk density. They investigated the precision, linearity for soil-like material, spatial resolution and limitations of CT using a fourth generation scanner at Michigan State University. Using glass beads and hollow glass spheres plus a sandy loam soil, they looked at beam hardening as influenced by sample size and relative density changes. Both the glass bead spheres and soil experiments showed a linear response of Hounsfield units, (H), to bulk density. The values of H ranged from -800 to +800 for the experiments. The results for the soil were more varied and had a lower correlation than for the glass bead spheres. Beads were 0.2 mm in diameter while the glass hollow spheres used to obtain low bulk densities were 0.1 mm. Containers used for the bulk density part of the experiment were aluminum, 7.37 cm inside diameter by 12.5 cm long. Wall thickness was 1.3 mm. CT scan parameters used were 125 keV, 30 mA, 12 second scan time and 10 mm wide x-ray beam (slice width).

The contrast/resolution part of the experiment showed that air-filled holes ($H=-1000$) within acrylic tubes ($H=125$) in the water-filled ($H=0$) aluminum container could be clearly detected down to a diameter of 1.25 mm with diameters of 1.00 mm being slightly visible but not separated from one another on the image produced at the CT scanner monitor. When the holes were filled with a glycerol/propanol mixture having an H value only about 1 percent different from water, the smallest hole detected was 6.4 mm in diameter.

Petrovic et al. (1982) also investigated the beam hardening artifact problem as it relates to density changes within the object. Using small stones they found that a 4 mm diameter stone within a water medium was accurately imaged, but a 6 mm by 12 mm stone caused an erroneously lower H within 3 mm of the stone. The maximum error in H was -8.5 percent. A 15 mm by 22 mm stone caused errors up to -20 percent within 5 mm and caused streaking of the image

throughout the container. When the stones were placed within the denser medium of glass beads, there was still streaking from the largest stone but the maximum error was -10 percent. Long, straight air-filled holes with long axis lying in the scan plane also caused lines or streaks in the image at the air-medium interface. They suggest that some CT scanners are better able to compensate for certain beam hardening artifacts than others and advise use of smaller diameter samples to minimize this artifact. They conclude that CT scanners are potentially useful for determination of soil bulk density and have good spatial resolution.

The authors did not report any experiments for detection of air-filled holes in denser medium such as the soil itself, but the greater the contrast, the greater should be the resolution or ability of detection of small holes. The greater variability using the sandy loam may have been due to actual variation in bulk density within the packed container.

Hainsworth and Aylmore (1983) used CT to determine the spatial distribution of soil water content. They point out the inherent advantages of the technique when compared to conventional techniques such as gravimetric sampling, and neutron or gamma probes. In addition to using x-ray CT they attempted to apply the CT principles to a gamma radiation source and detector by taking multiple views through a soil by turning the soil container rather than rotating the source/detector around the sample. The x-ray CT scanner used was a first-generation model with pixel resolution of about 1.5 mm by 1.5 mm. Slice width was 10 mm and peak voltage was 120 KeV. They used three 70 mm tall concentric acrylic cylinders with different soil water contents in each ring. In addition a 0.6 mm inside diameter alundum tubing was inserted through the soil in a 70 mm diameter Perspex pot packed with soil to function as a linear source for water in order to assess the ability to determine water content under dynamic conditions. A radish was planted in another pot to determine soil moisture distribution around and movement to a root after periods of 7 and 20 days.

They derived an expression for the attenuation value, μ , for wet soil as follows:

$$\mu_{\text{wet}} = \mu_s \rho_s + \mu_{\text{water}} \theta_v \quad (2.2)$$

where

μ_{wet} is the mass attenuation value for wet soil,

μ_s is the mass attenuation value for solids,

μ_{water} is the mass attenuation value of water,

ρ_s is the soil bulk density, and

θ_v is the volumetric water content.

For a perfectly dry soil

$$\mu_{\text{dry}} = \mu_s \rho_s \quad (2.3)$$

Combining Equations 2.2 and 2.3

$$\theta_v = \frac{\mu_{\text{wet}} - \mu_{\text{dry}}}{\mu_{\text{water}}} \quad (2.4)$$

and using Equation 2.1 for Hounsfield units, they obtained an equation in terms of Hounsfield units, H

$$\theta_v = \frac{H_{\text{wet}} - H_{\text{dry}}}{1000} \quad (2.5)$$

This equation provides for the calculation of water content on a volume basis when the underlying dry bulk density is known. It should be valid on a pixel-by-pixel basis of the scanned cross section of the soil or on an average basis for a group of pixels. The H_{dry} value(s) would have to be determined by a previous scan or by assuming a uniform packing arrangement, particle density and attenuation coefficient for the material.

Results of the experiments showed that the x-ray CT scanner, on the average, accurately determined the soil water content when compared to gravimetric determinations of water contents in the samples. However the scanner slightly overpredicted the water content in the outer ring and slightly under predicted in the middle ring. The authors first attributed these results to the Gibbs phenomenon which results from large changes in density within an object and causes the calculated μ values in the low density area to be less than the actual μ for that area (Brooks and Di Chiro, 1976). However after careful examination of the data, they felt that the limiting of the spatial frequencies in the Fourier transform used in the reconstruction algorithm was at least partly the cause. They made this conclusion based on the width of the pixels where the effect was seen and the fact that there were stepped increases in θ_v , making the spatial limiting of the Fourier transform more problematic. Proper filtering of the x-rays at the source may help prevent the Gibbs phenomena from occurring.

Large standard deviations on the order of 20 H (corresponding to 0.02 g cm^{-3}) was found in the values of θ_v for the concentric rings but some of the variation could have been due to natural variation in the dry bulk density which was not measured by the scan method prior to addition of water. The standard deviation for θ_v in the case of the artificial root (alundum tubing) was 0.006 g cm^{-3} . Results of the gamma source CT scanning were mixed as there were initial problems with the source materials tried. Cesium-137 proved to be relatively insensitive to small water content changes over small distances and gave nonlinear attenuation coefficients for some instances of material thicknesses. Other sources such as americium-241 were limited due to self absorption and low maximum photon output resulting in long count times for each projection (about 90 minutes). Other sources have low half-lives limiting their effective working life.

In a followup and similar study Hainsworth and Aylmore (1986) used 16 pots with radish roots established to test different theoretical concepts regarding water flow to and near roots. They were of the opinion that there was a need for an accurate method to test the theories that had been developed and saw x-ray CT scanning as a possibility. Soil in pots was scanned dry and then at frequent intervals at the same cross sections to help eliminate the problem of inherent deviation in dry bulk density. Dry bulk density was assumed to remain constant during the experiments, although some compaction of soil around the growing root is possible. Some evidence of slight compaction by the root was seen. The authors concluded that x-ray CT accurately determined the spatial and dynamic changes in water content in the pots and offered an exciting new approach to resolve some controversies regarding water extraction by plant roots.

Crestana et al. (1985) used a GE third generation scanner to study the dynamic movement of water in soil. Using a peak voltage of 120 keV, they scanned eight samples of two soils at different bulk densities to obtain a calibration curve for bulk density and then scanned nine samples packed to a given bulk density with different water contents to obtain relationships for changes of Hounsfield units with water content. They also scanned soil samples as water was applied to the sample from one surface in order to determine the rate of water movement and changes of water content at different depths in the soil. They scanned about every 5 seconds at the same position for the dynamic analysis. Linear relationships for bulk density and water content were developed in the calibration portion of the experiment. The dynamic portion showed the ability of the scanner to detect water movement in the column at a rate of 1.6 mm per second and revealed the rapid changes in water content as a wetting front moved through the soil column. They conclude that x-ray CT scanning opens new possibilities for nondestructive measurement of the spatial and dynamic water contents in soil. They suggest that a much simpler CT instrument could be inexpensively constructed for use in the field of soil science which would overcome the shortcomings of the conventional CT scanners designed specifically for the medical field.

In a study using porous foam media, Brown et al. (1987) attempted to eliminate any variation of attenuation values due to spatial density changes of the dry media itself. They used a third-generation scanner operating at 120 KeV, 120 mA, 3.0 second scan time and 1.5 mm slice width. Three porous phenolic foam materials were cut into blocks, scanned dry, saturated and then scanned after 16 hours of drainage. Cores 10 mm apart were taken along the vertical axis of

the media for gravimetric determination of water content. Results showed reasonable but not total agreement between the gravimetric and CT determined water contents. The authors felt the CT scan process had an accuracy within plus or minus one percent. Absolute values of the differences for the two methods were as high as $0.09 \text{ m}^3 \text{ m}^{-3}$ but averaged about $0.013 \text{ m}^3 \text{ m}^{-3}$. The dry bulk densities of the foam media used varied from 12.1 to 16.7 kg m^{-3} and had water contents at saturation from 0.88 to 0.94 on a volumetric basis. The attenuation values at oven dry were from 16 to 24 in **H** units. There was considerable variation among the water distribution patterns of the three materials as shown by both the gravimetric and CT methods. Attenuation values at saturation varied from 480 to 525 in **H** units.

The differences could perhaps be explained by the different sample volumes and sample locations used for the two methods. As can be seen, the water content was a high percentage of the total mass. Consequently, the attenuation due to water in the samples was a much greater part of the total attenuation than that due to the relatively low density materials. The differences among the three materials in water holding capacity in the vertical plane and the variation given by both methods leads to the question of whether the variation in values (and differences between methods) could be due to nonhomogeneity within the materials. How the results pertain to much denser media such as soil is also a question.

CT had been used by Tollner and Verma (1987) and Tollner and Ramseur (1988) to assess its application to measurement of soil moisture and bulk density. The scanner used in these studies was a EMI 5005. Parameters used were 120 keV, 1881 MAS (33 mA x 57 sec), 320 mm diameter scan field, and a 5 mm slice width. The resulting pixel size was 1 mm by 1 mm. In the 1987 study a medium coarse silica sand was packed into two side by side 22.5 cm deep by 7 cm thick by 9 cm wide compartments within a plywood container. This container was placed inside a plywood cylinder in order to present a circular cross sectional shape to the scanner. The mean dry bulk density of the sand for each compartment was 1.505 Mg/m^3 . The container was scanned at four location under the following conditions: 1)...with the dry sand, 2). after allowing the sand to saturate slowly, and 3). after drainage from the saturated condition for 1, 2, 3 and 6 days. After the final scan gravimetric moisture samples were taken from each compartment at 5 depths below the soil surface.

Mean and variance values of Hounsfield units (**H**) were obtained for circular regions with radii = 15 mm within the sample, corresponding to the physical sample positions for each scan. Although the average of **H** for all regions for the dry condition were nearly identical for each compartment, there was considerable variation among the different regions. Coefficients for equation 2.1 were obtained for each compartment using the physical samples and the **H** values after day 6. Values of R^2 were 0.92 and 0.89 for the left and right compartments respectively. There was considerably more variation of **H** values for regions in the right side than the left side for all scans.

The authors state that these variations could be due to actual differences in bulk density (or moisture content), but believe that artifacts were more likely causing the variation since there was more variation in the dense medium of sand than a standard calibration using water. They state that artifacts can be a significant limiting factor in making quantitative measurements in x-ray CT, especially with denser media and with containers with sharp corners. As the authors indicate, improvements in scanner hardware and reconstruction algorithms will help reduce artifact problems in CT scanning. They advocate the need for replication in scanner studies, saying that it may not solve the artifact problem but the degree of variation may indicate the presence and severity of artifacts.

Through out their correlation analysis, the authors are assuming that there is no actual differences in bulk density within either compartment or soil moisture differences at a given depth. They attribute the greater variance in the dense medium than in the calibration standard to artifacts, but it would seem that there would inherently be more variation in a packed solid particle medium than a liquid medium. Although the rectangular container was placed within the cylinder, there may be more artifact problems than with cylindrical containers. The consistently greater variation in the one side for both dry and wet conditions may indicate actual differences in bulk density due

to differences in pore sizes from nonuniform particle sizes, packing inconsistencies, or bridging of particles. Differences in pore sizes would affect not only the dry bulk density, but also the moisture retention characteristics under unsaturated conditions, thereby compounding the variation.

In the 1988 study (Tollner and Ramseur) a sandy loam soil was compacted at a moisture content of 16.75 percent (db) to different average bulk densities in five, 110 mm diameter by 140 mm high plastic containers. Containers were scanned at three locations for the initial moisture and for five moisture contents after successive drying periods in an oven. In addition a soybean plant (*Glycine max*) was planted in soil within a 200 mm diameter PVC pipe and scanned three times per week for a month.

Results showed that x-ray absorption prediction using linear bulk density and volumetric moisture terms in a regression equation had an R^2 value of 0.99. Quadratic terms for either bulk density or volumetric moisture did not significantly improve the regression. A cross product term of the two independent variables was significant but only slightly improved the R^2 value. The significance of the cross product term suggested an interaction between the bulk density and moisture content. The authors suggest that it was due to shrink/swell phenomena of the soil, saying that the soil exhibited some shrinkage on drying.

In assessing the impacts on the variation of attenuation, the authors found that the solids' bulk density had a far greater effect on standard deviation of pixel values than did moisture content. The quadratic term of bulk density was significant for prediction of standard deviation. The authors do indicate that scanning at an air-dry condition showed some variation. They attempted to compensate for this variation by calculating bulk density for each position and assuming it remained constant for the entire study. In other words they assumed that any variation in values for the initial scan were entirely due to real dry bulk density differences and that any changes with successive scan were only due to changes in moisture content within the pixel. There was a wide range of water content measured with the scanner for the growing root, but the one gravimetric sample taken from one position agreed well with the scan predicted value for that position at the end of the experiment.

The significance of the quadratic term of bulk density and not of water content for prediction of standard deviation should not be surprising since the attenuation is primarily a function of mass density, and the solids in the media have a much higher density than water. In fact if the percent of voids was 50 percent and the specific gravity of the solids was 2.65 as is typical for silicate material, the impact of the solids would be 2.65 times greater than that of the water for the saturated condition. The impact would be even greater for unsaturated conditions. Any actual variation in bulk density due to uneven packing would be expected to give significant variation in pixel attenuation values. Any bulk density changes due to shrink/swell or compaction from the growing root were evidently ignored. It should be remembered also that the linear attenuation coefficient is made up of the coefficients for two or more interaction processes which possibly could lead to nonlinear terms in a regression equation.

Wang (1983) used CT to analyze multiphase flow through porous media. A second generation CT scanner was used to determine unstable wetting fronts or fingering when a displacing fluid (water) was injected into a small grained sand or a glass bead medium saturated with oil. The study also looked at the variation in attenuation coefficients with size of holes in a dense medium. Four holes (0.64, 0.32 and two 0.16 cm in diameters) were drilled in a sandstone core which was scanned. Results were given in the form of a three dimensional graph showing the relative differences in coefficients. There were differences with size of hole but no absolute values were shown. The pixel size of the system used was 0.8 mm.

He assumed that if the atomic composition and photon energy spectrum are constant over a cross section then the linear attenuation coefficients are only related to the physical densities of the volume elements (pixels). Furthermore, if each element consists of solid particles and combinations of fluids occupying void space, then the average linear attenuation coefficient for a pixel is given by:

$$\mu_{i,j} = (1 - \phi_{i,j}) \mu_{\text{solid}} + \phi_{i,j} \mu_{\text{fluids}} \quad (2.6)$$

or for the case of the two fluids oil and water:

$$\mu_{i,j} = (1 - \phi_{i,j}) \mu_{\text{solid}} + \phi_{i,j} [(1 - x_{i,j}) \mu_{\text{water}} + x_{i,j} \mu_{\text{oil}}] \quad (2.7)$$

where

$\phi_{i,j}$ is the void fraction of the porous medium,

i,j represents the i th row and j th column of the matrix, and

$x_{i,j}$ is the volume fraction of the oil occupying the void space.

A homogeneous medium was assumed for the very fine grained sandstone. Therefore the void space, $\phi_{i,j}$, was assumed constant over the scan. From the observed attenuation coefficients, the $x_{i,j}$ for the scanned matrix could be calculated, given the values of μ_{air} and μ_{water} .

Anderson et al. (1988) used CT to measure a range of bulk densities for two soils (Cridder and Mexico) composed of different materials. The two soils were shown to have different attenuation values for the same volume fraction, and different slopes of attenuation coefficients plotted against fraction of solids. The authors explain that the difference for a given volume fraction is explained by the higher iron content of the Cridder soil, but state "It is not known why this (the nonparallel lines) occur because theory says the two slopes should be parallel".

One explanation for the nonparallel slopes is that the number of electrons per unit volume is increasing at a greater rate for the Cridder soil (with the high iron content) than for the Mexico soil. As the volume fraction of solids is increased, the mass per volume (bulk density) increases more for the Cridder than the Mexico soil due to the higher particle density. As the authors indicate, the attenuation coefficient depends on the electron density. The attenuation of an x-ray is proportional to the number of electrons available for interaction by the x-ray beam as it passes through a material. Electron density can be either on a mass basis, i.e. the number of electrons per unit mass, or on a volumetric basis, i.e. the number of electrons per unit volume of material (McCullough, 1975). The applicable usage for CT is the volumetric basis since the attenuation coefficients are calculated for pixels having physical dimensions.

The non-zero intercept for the regression equations for the relationship between the attenuation coefficient and the volume fraction of soil solids mentioned by Anderson et al. (1988) may be due to use of a polychromatic source, to significant coherent scattering and photoelectric effects or to multiple solid constituents with differing attenuations in the soil. Although the Compton effect would be the dominate interaction at the peak voltage of 120 keV used in the study, the presence of the other effects would produce an overall nonlinear relationship. The potential for these factors and their impacts are addressed in the next section.

2.3 Discussion.

Several physical limitations have been built into the CT scanners commonly found for use in the medical field. The x-ray dose (both rate and total amount) given to a human patient is critical. Consequently the CT scanner has been designed to limit the voltage and number of projections that is available during operation. Total scan time has also been limited in order to avoid problems with patient motion, either voluntary or involuntary. This potential problem is not a concern with inanimate objects encountered in soil science, although it should be considered for dynamic studies of water movement.

In particular the polychromatic energies with a peak voltage of approximately 125 keV commonly found in medical CT scanners are not optimal for use with soil or other dense material. Data from Hubbell (1969) shows that a monochromatic energy between 150 keV and 1,020 keV would be much more suited since both the scatter and photoelectric interactions are negligible, but pair production is still not a factor. Energies in this range cannot be attained with x-ray tubes but are only produced as gamma rays from decaying isotopes. A number of researchers have used gamma radiation to measure both water content and soil bulk density, including use of dual-energy systems (Stillwater and Klute, 1988).

Calculation of matrix attenuation values and reconstruction of the image have also been optimized for medical uses. Medical scanners are designed to produce almost instantaneous image

reconstruction in order to provide immediate review to determine the need for further scans of a patient. Consequently, the algorithms used to calculate the individual pixel attenuation values must be very fast. Since in the medical field the CT scanner is used mostly for qualitative versus quantitative results, accuracy or resolution can be sacrificed for speed. In soil science or similar fields where accuracy and high resolution are more important than speed. Images could be formed at a later time from the raw data, allowing more accurate algorithms and reconstruction methods to be used.

3 STUDY METHODOLOGY

3.1 Specific Objectives.

The general objective of this study is to evaluate the use of CT to directly and nondestructively characterize macropore structure in soil columns. Two areas of research to be addressed are: first, the ability of a CT scanner to detect naturally occurring macropores in a dense medium such as soil, and secondly the quantitative accuracy of the size, shape, position and attenuation values of the air-filled holes that are detected. Field cores were taken and scanned to address the first area to see if distinctions of macropores in the soil could be seen in the CT images produced. The quantitative problem must be addressed by scanning samples with "macropores" of known size and shape. Packed samples of "soil" with artificially produced macropores were made and scanned to address this problem. Specific tasks that the research attempts to address are:

1. Assess the ability of CT to qualitatively detect and image holes within soil,
2. Determine the optimal CT scan parameters for detection of air-filled macropores in soil,
3. Determine the size of hole that can be detected by a medical CT scanner,
4. Develop a method of determining the size and shape of macropores from CT scan data,
5. Assess the ability to determine the connectivity of macropores with depth in soils,
6. Compare the CT scan method with other methods of macropore characterization, and
7. Develop recommendations for CT analysis of soil samples.

The methods used to address these specific tasks are described in the following sections of this chapter.

3.2 Field Cores.

Soil samples to use for the detection of naturally occurring macropores were obtained by taking cores from field areas where macropores were thought to exist. The objective was to obtain cores that were undisturbed as much as possible in order to have representative samples of the natural conditions. Field cores were obtained from agricultural research plots located on the Agricultural Experiment Station farm located in St. Paul, Minnesota. Three different cores were taken. The first two cores were taken from an uncultivated area between a cultivated field and a field road that had been vegetated with Kentucky bluegrass (*Poa pratensis* L.) for many years. The only cultural practice was periodic mowing of the grass. The third core was taken from a small bare area within the end rows of an adjacent tilled field that was in corn (*Zea mays* L.). The location of the third core was approximately 10 m from the location of the grassed cores. Conventional tillage and continuous row crops had been practiced in the field for at least 15 years. All cores were taken in June, 1987 during a period of heavy rains in the area. Soil moisture was near field capacity.

The soil from which all three cores were taken was a Waukegan silt loam (fine-silty over sandy or sandy skeletal, mixed, mesic, Typic Hapludoll). These soils are characteristically well drained with moderate permeability and have a weak fine subangular blocky structure in their top horizons. Field slopes at the site are less than two percent.

Core 1 (from the grass-surfaced area) was excavated by carefully digging around an area about 200 mm in diameter to a depth of about 300 mm using a spade. The core was then cut off at its base, and placed in a plastic bag. The columnar shape of this core was maintained by careful handling. Cores 2 and 3 (grassed and tilled areas respectively) were obtained by driving a PVC (polyvinyl chloride) pipe (nominal diameter of 203 mm) into the soil in increments of about 100 mm and then digging around the outside of the pipe. This process was repeated until a total depth of about 700 mm was reached, after which the column was cut at its base and removed from the hole. Figure 3.1 is a schematic of the collection technique for Cores 2 and 3.

Surface sealing due to the recent heavy rains was evident at the surface of Core 3 (tilled field), but there was no evidence of macropores such as earthworm holes, root holes and cracks at the surface. Surface sealing was not evident in Cores 1 and 2 (grass surface). A few earthworm casts and small holes were found after removal of the grass cover. Later examination of the cores showed the presence of ant colonies within both cores taken from the grassed area. Melted

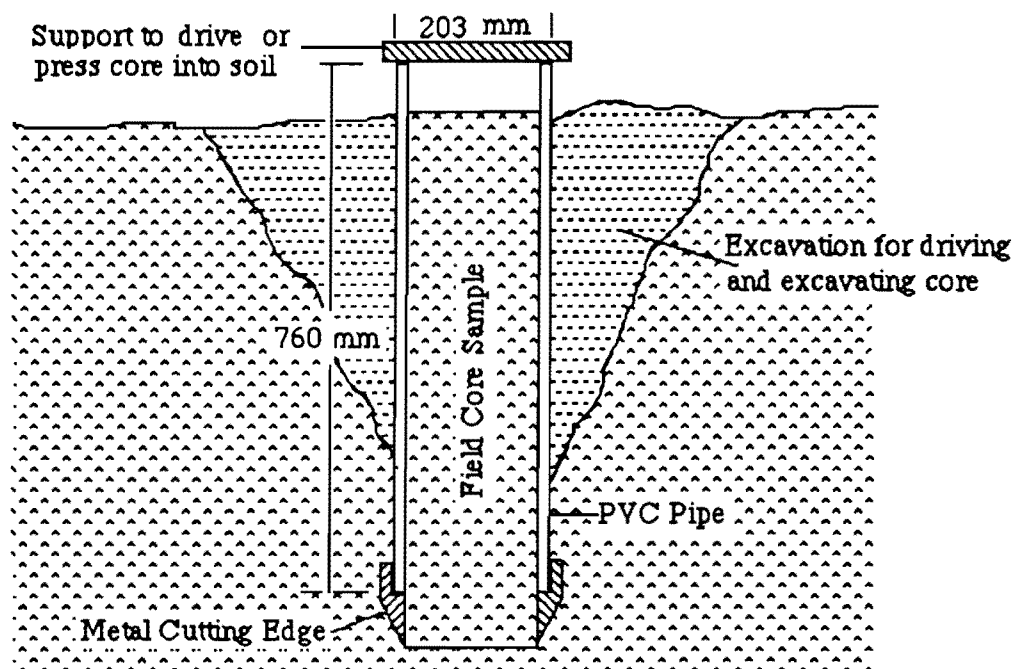


Figure 3.1 Schematic of Field Core Collection Technique Using PVC Pipe.

paraffin was poured around the top inside circumference of the cores to seal off any flow along the core walls during dye tracing experiments. The ends of the PVC pipe were covered with polyethelene to prevent loss of material during the scanning process.

The PVC $[(C_2H_3Cl)_n]$ pipe was chosen for the cores because it has a fairly low attenuation coefficient but yet is strong and rigid for driving into the ground. Steel pipe with a high iron content ($Z = 26$) has a high and nonlinear attenuation coefficient due to the large photoelectric effect. The presence of steel usually causes artifacts in CT scanning. Aluminum pipe ($Z = 14$) might also be a suitable material but has a density twice that of PVC and would therefore absorb more of the x-ray energy. It also would be more expensive. The linear attenuation coefficient of PVC is about half that of aluminum (White, 1978). The pipe was sharpened on one end and driven into the ground with a sledge hammer. There was some jarring caused by this method, and it possibly caused some cracks to form in the cores. In later applications, a cutting edge was made that would fit over the end of the pipe, eliminating the need to sharpen the pipe and reducing the resistance to driving into the ground. In addition the inside of the pipe was coated with petroleum jelly and the outside was sprayed with silicon to reduce the resistance. The hydraulic bucket on a tractor was used instead of the sledge hammer to push the pipe to avoid the jarring impact of the hammer.

The size of pipe was selected based on the need for a large enough sample to adequately represent the distribution of macropores to be measured, yet small enough to be handled when full of soil. The size selected (8 inch nominal outside diameter or 203 mm) turned out to be advantageous in the scanning process. The scanner used had two possible fields of view, one of 530 mm diameter for a whole body scan and 250 mm diameter for a head scan. The smaller field of view accomodated the pipe and resulted in a pixel size of approximately 0.5 by 0.5 mm versus a 1.0 by 1.0 mm size for the larger field of view. The 203 mm diameter of the pipe is two to three orders of magnitude greater than the 0.5 mm pixel size. This size of pipe should therefore be large enough to be a representative sample for the size of macropores that could be detected by the system. In addition, it should be adequate to assess any lateral, i.e., horizontal, changes in location of individual macropores. The length of pipe used of about 700 mm was based on the practicality of driving the pipe that deep and of handling the pipe full of soil. Total weight of the pipe filled with moist soil was 40 to 45 kilograms.

3.3 Packed Cores as Standards.

Two packed soil columns with artificially produced macropores were scanned as standards. The objectives were to determine the accuracy with which CT portrays the size and location of known macropores within different porous media and to determine the attenuation coefficients for various soil components. The first column consisted of a 105 mm long section of 203 mm diameter PVC pipe packed with dry fine sand having a specific gravity of 2.67. The dry bulk density of the sand medium was 1.69 g cm^{-3} . Glass tubes of various diameters were inserted at angles of 90, 45 and 22.5 degrees from the scan beam to assess the ability to detect macropores at various orientations. In addition, two plastic tubes (drinking straws) with inside diameters of 7.14 mm (9/32 in) were included at right angles to the scan beam. The low density, thin-walled plastic straws serve as a comparison with the relatively dense, thick-walled glass tubes. The plastic straws had been perforated in order to offer the opportunity to add water or other fluids to the standard. Figure 3.2 shows the hole number, angle and location of the different tubes, and Table 3.1 provides information regarding the size of each tube.

The second standard consisted of the same size PVC pipe as for the first standard (sand), but was packed with the Waukegan soil to a dry bulk density of 1.21 Mg m^{-3} . The soil was dried, sieved to 1 mm or less in size and packed in layers into the pipe. Water was added to the soil to facilitate the packing process. The moisture content after the addition of the water was 26.8 percent (weight basis) resulting in an average wet bulk density of 1.65 g cm^{-3} . Holes varying in diameter from 0.90 mm (0.035 in) to 9.5 mm (3/8 in) were formed longitudinally along the column by the inclusion of plastic tubing or steel rods of different diameters during the packing of the soil. The steel rods were carefully pulled out of the column to form holes while the plastic tubes were left in the column during the CT scans. Figure 3.3 shows a schematic of a cross section of the packed column, locating the position, size and type of the different holes and tubes.

3.4 CT Scanner Parameters.

The CT scanner used in this study was a Siemens SOMATOM DR3 located at the University of Minnesota Hospital. This scanner is a commercially-available, third-generation medical scanner with a pulsed, fan x-ray beam and 514 rotating detectors. The two outside detectors are used for calibration, leaving 512 detectors for collection of scan data. The operating system uses version F2 software. Image reconstruction time is from 0 to 3 seconds and scan times vary from 1.4 sec to 14 seconds depending on the number of views or projections used. The number of views can be set to 240 or 320 for a rotation of 240 degrees around the object or 480, 720 or 1,440 for a rotation of 360 degrees. As there was no concern for the total amount of radiation, the number of views used for all scans in this study was 1,440 in order to produce high detail, low noise images. Each view corresponded to 0.25 degrees of rotation by the x-ray tube and detectors. Attenuation values for each pixel were calculated from the projection data using a high resolution, edge enhancing filter that is proprietary to the system. The scan time corresponding to this number of views was 14 seconds. The energy used for all scans for the field cores and packed column was 125 peak kilovolts. The actual energy of the photons is polychromatic and will fall within a range of 30 to 125 keV. Heat units of 700 milliampereseconds were used for the scans.

The gantry opening on the DR3 scanner is 540 mm in diameter, with two settings for the tube-to-detector distance. Resultant fields of view are 530 mm and 250 mm for the two settings. The 250 mm field of view was used in this study as mentioned above and results in a matrix of pixels 512 by 512 in number. Slice width can be set at 2, 4 or 8 mm. The 2 mm slice width was used for all the scans in the field cores while both 2 and 8 mm widths were used in the packed columns. As explained in Section 4.4, the 2 mm width has the advantage of providing the greater detail where partial volume effects may occur due to angling macropores. However, it has the disadvantage of producing "noisier" data than an 8 mm slice for a uniform macropore at a right angle to the scan beam. The smaller slice also requires more scans to completely scan a distance along the sample. The potential problems of the 8 mm slice width for the case of angling macropores are analyzed using data from the sand standard with the glass tubes at different angles.

The field cores were scanned at varying distances along their longitudinal axis, i.e. depth into the soil profile. An approach of obtaining representative scans at varying depths was used rather than attempting to make scans at every point along the axis. Scanning the entire depth of the 700 mm deep cores with a slice width of 2 mm would have required 350 scans which would have proved prohibitively expensive in both machine time and analysis time. A distance between scans of 10 mm was selected for the top 100 mm of the field cores, 20 mm for the middle portion (100 to 300 mm) of the cores and 50 mm for the lower part of the cores. The smaller increments were used near the top of the cores because there was greater variation with depth near the surface. Both soil density and the number of macropores changed more rapidly in the upper portions versus lower portions of the profile. In the case of the packed standards, scans were taken at 5 locations at 10 mm increments along the longitudinal axis.

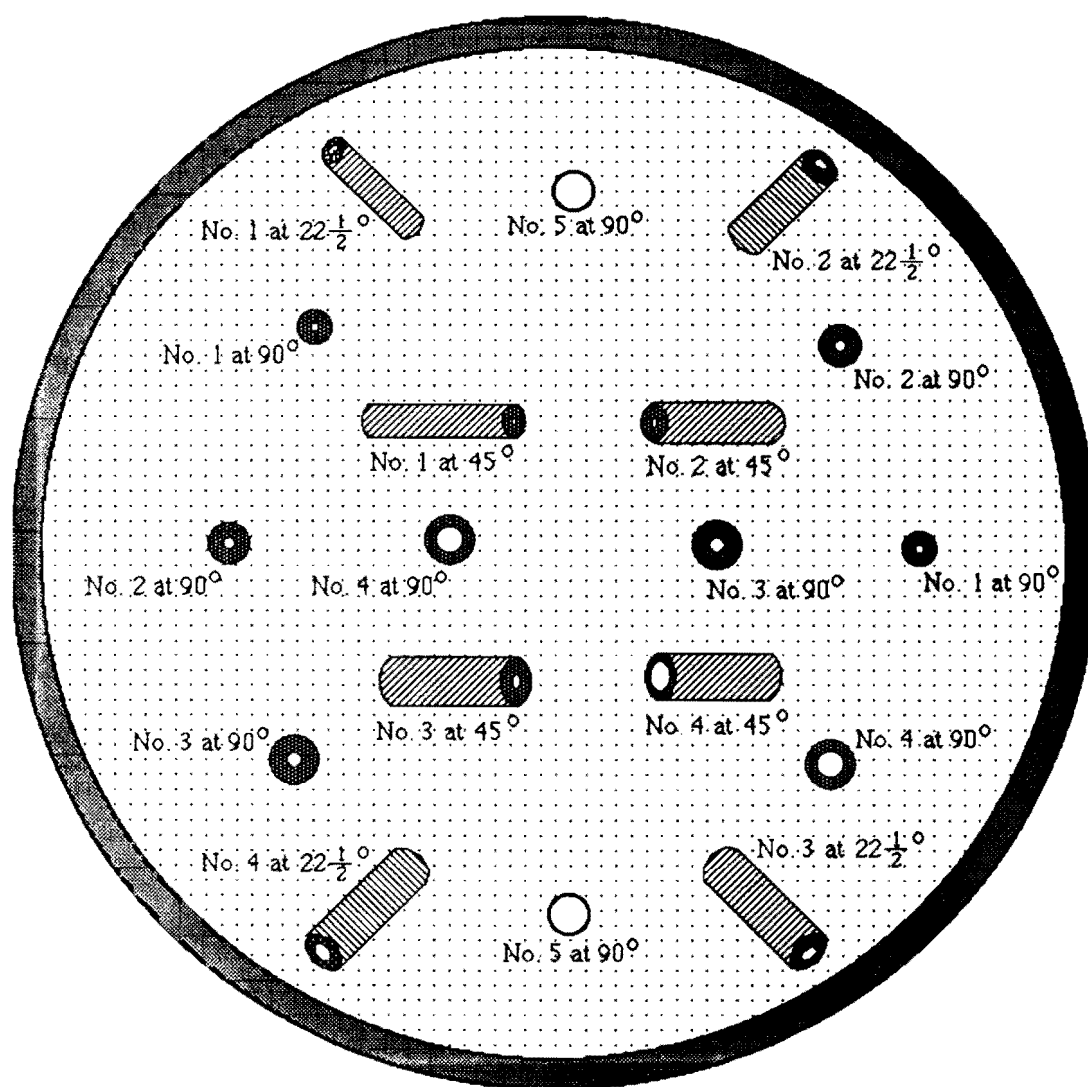
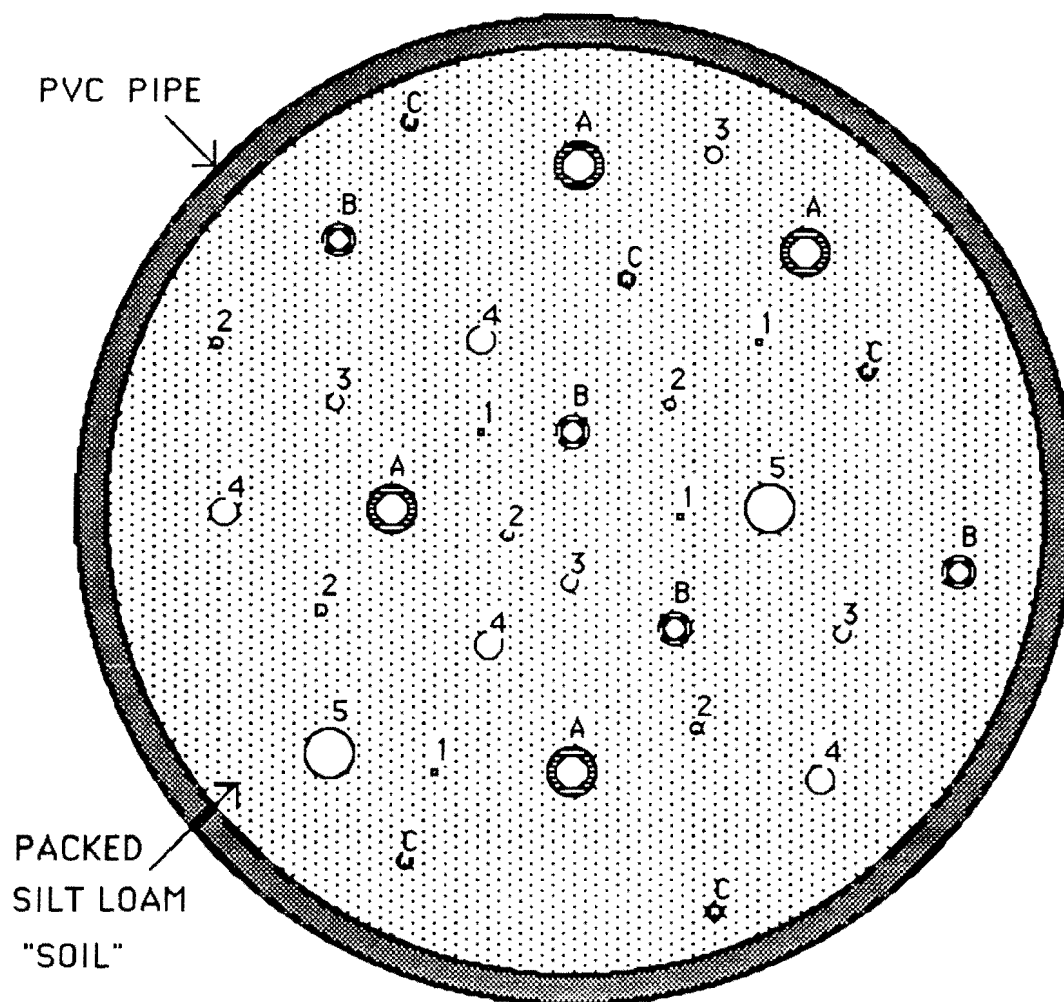


Figure 3.2 Schematic of Sand Standard with Artificial Macropores.

Note: See Table 3.1 for explanation of hole numbers.

Table 3.1 Type and Size of Tubes Used in Sand Standard.

Hole No. in Fig. 3.3	Hole Type	Inside Diameter mm	Outside Diameter mm	Area mm ²
1	Glass Tube	0.90	6.50	0.64
2	Glass Tube	1.90	7.50	2.84
3	Glass Tube	2.90	8.90	6.60
4	Glass Tube	4.80	8.90	18.10
5	Plastic Straw	7.14	7.37	40.08



Key to Letters and Numbers:

- A: Plastic Tube, 0.250 in. Inside Diameter, 0.375 in. Outside Diameter.
- B: Plastic Tube, 0.166 in. Inside Diameter, 0.250 in. Outside Diameter.
- C: Plastic Tube, 0.096 in. Inside Diameter, 0.120 in. Outside Diameter.
- 1: Hole formed by metal rod, 0.90 mm (0.035 in.) Diameter.
- 2: Hole formed by metal rod, 1.59 mm (0.0625 in.) Diameter.
- 3: Hole formed by metal rod, 3.18 mm (0.125 in.) Diameter.
- 4: Hole formed by metal rod, 4.76 mm (0.188 in.) Diameter.
- 5: Hole formed by metal rod, 9.52 mm (0.375 in.) Diameter.

Figure 3.3 Schematic of Silt Standard with Artificial Macropores.

3.5 Image Display and Analysis.

Individual scan data are reconstructed into an image that can be displayed on a black and white, CT-dedicated monitor. This is done automatically by the scanner-dedicated computer and allows display of the image within a few seconds of obtaining the scan. Images can also be obtained on photographic film at various scales as a permanent record. In addition the pixel by pixel data for each image can be saved on magnetic tape for redisplay of the images at the monitor at a later time.

Images can be manipulated at the monitor to accentuate features by changing the window and/or center "brightness" values used for different display shades. The window and center values are in Hounsfield units which are obtained by subtracting the attenuation value of water from the attenuation value for the pixel and dividing by 1000 (Brooks and DiChiro, 1983). The Hounsfield unit for water is therefore zero. The window is the range of values covered by the shades of gray, while the center value is the median value for the range. For example, if the window is set at 1600 and the center value at 200 and there are 8 shades of gray used, any pixel with a Hounsfield unit less than -600 would appear black while any pixel with a value above 1000 would appear white. Pixels with values between -200 and 1000 would be assigned 8 shades of gray (from black to white) in equal increments of 200 Hounsfield units.

Actual Hounsfield units for specific points on the image can be obtained at the monitor by use of a screen pointer or wand. However, a distribution of values for exact locations or the entire scan is difficult to obtain from the CT dedicated monitor. In addition access to the CT dedicated monitor at commonly available scanners is usually limited due to the priority for medical use. To overcome these problems, scan data for Cores 2 and 3 and the standards were saved on magnetic tapes, loaded onto a main frame computer at the University of Minnesota Computer Center and downloaded to a microcomputer.

Data for each scan consist of an attenuation value for each pixel. For the scanner used in this study, values are stored as positive integers using a low byte and high byte format for each pixel attenuation value. The pixel value as a positive integer is obtained by multiplying the high byte value by 256 and adding the low byte. The value in Hounsfield units is equal to the stored pixel value minus 1024. Byte values are stored as hexadecimal numbers. For the 512 by 512 matrix of pixels, there are 512 by 512 by 2 bytes or 524,288 bytes of information. An additional 256 bytes is used for the header information giving the date, number, and scanner parameters of the image. Resultant file size for each image is 524,544 bytes.

Programs were developed whereby images could be recreated from the data and displayed using either black and white or color-coded ranges of attenuation values on microcomputers. The image programs were developed by Deborah J. Hansen, Senior Applications Programmer for the Department of Agricultural Engineering, University of Minnesota. The image programs were written in Turbo Pascal™ for both IBM (AT and PS/2 or compatible) and Macintosh II computers. Further information regarding the image display program is given by Warner and Hansen (1989) and Warner (1990).

3.6 Sectioning of Cores.

The outside of the PVC pipe for Cores 2 and 3 was marked at the location of each scan. The "front" or topside of the pipe in its horizontal scanning position was also marked so the cores could be sectioned at the location of the scan images and referenced to the images. The cores were sectioned about one week following drainage from some infiltration and dye experiments. Consequently, the cores were near field capacity in water content when sectioned.

Various methods for sectioning the cores were evaluated. These included the use of hand and power saws, a large machine lathe, fine wire, sharp knives, and sawing after freezing the core. However, all these methods smeared the soil making detection of macropores difficult. The best method found was to first saw through the PVC pipe with a hack saw at marked scan locations and then break or manually shear the soil at that location. Manual shearing did not smear the soil but

had the disadvantage of at times producing an uneven break along the desired plane. When uneven breaks occurred, a straight pin and a chisel were used to produce a clean break in the vicinity of the scan plane. A shop vacuum cleaner was used to remove loose particles on the soil surface that might cover macropores.

After obtaining a fairly even surface, coded colored pins were stuck into the surface of each section to identify holes, cracks, roots, stones and filled holes (plugs). Stained features such as holes and roots were differentiated from unstained features. Photographs of each section were taken with and without the pins. The sections were visually compared with the CT scan images at those sections to determine if the macropores shown on the images coincided with those in the sections. A more in depth verification of the accuracy of the scan process was done using the images of the two packed soil columns or standards as described in the next section.

The connectivity of various macropores to the surface was assessed by the presence of dye in successive photographs. In addition, after dividing Core 2 into two equal lengths, a very fine sand was poured into two large macropores, about 7 mm in diameter, appearing at the ends of each section to assess the continuity of those macropores.

3.7 Analysis of Data from Silt and Sand Standards.

Scan data from the two standards were used to test the accuracy of the CT scanner in determining the size of holes. The value for an air-filled hole was investigated in order to determine the proper value for the characterization of macropores in the field cores. Due to the boundary and partial volume effects described in Sections 4.7 and 4.4, the attenuation values for air may not be the same from hole to hole. Therefore, the air-filled attenuation value was investigated for holes of various sizes in the two standards. In addition, the variation in size as measured for the same sized holes, both within the same standard and between the two standards was analyzed. The variation in the air attenuation value with the size of hole required that the effects of using different maximum attenuation or threshold values for air for the detection and sizing of holes be investigated. Three different threshold values were tested to determine the effect on size of hole detected and on calculated area of a hole. The threshold values used were 1024, 1124 and 1224 which correspond to H equal to -200, -100 and 0 respectively.

The glass tubes in the sand standard were particularly useful for this purpose because they had been precisely machined to given dimensions. The impact of the material density surrounding a hole was addressed by comparing values for a 4.8 mm hole in the silt standard and a 4.8 mm inside diameter glass tube in the sand standard. Comparisons were made between the 2 mm and 8 mm slice widths for scans made at the same locations within a standard to assess the importance of boundary and partial effects for holes, both at right angles and at oblique views to the x-ray beam. These analyses of the holes in the standards were made using a characterization algorithm programmed on the Macintosh II as described in the next section.

3.8 Quantitative Characterization of Macropores.

Two methods were used to determine the number of macropores within in certain size ranges in the field cores. First, color-coded displays on an IBM-AT were used to visually count the number and determine the size of each macropore shown on the image. The size for each macropore was determined by counting the number of contiguous pixels having an attenuation value less than the threshold value for air. A threshold value of $H = 0$ was used for this purpose. The pixel size was determined by counting the number of pixels corresponding to the known diameter of the PVC pipe. Once the area represented by one pixel was known, the actual size of individual pores could be calculated. This distribution was done for each scan of Core 2 only, and shows how the number of different sized pores changes with depth for that core.

The second method determined the size distribution of macropores using a computer algorithm to characterize individual holes. The program was written in Turbo Pascal for the Macintosh II and determined the location, size and a shape factor for each macropore found. The program uses file pointers rather than data arrays to find the value of individual pixels and their location with respect to adjacent pixels. This approach is used because the 512 by 512 array requires too much memory. The program first asks for input scan data file and the radius and

center coordinates (x, y) to describe the circle within which to look for holes. These parameters are obtained from the image display on the Macintosh II and are usually the same for scans of the same sample if it had not been moved between scans. The radius chosen for analysis of the field scans was approximately 10 mm less than the inside radius of the PVC pipe in order to eliminate any macropores near the edge of the scans that may have been formed by the sampling process.

The algorithm begins by searching left to right across each row until an attenuation value less than or equal to the chosen threshold value for an air-filled hole is found. The first value found corresponds to the left most pixel in the top edge of the top-most hole in the image. When it is found, the algorithm notes the location and keeps searching to the right to find the end of the top row and then "marks" the succeeding pixel in the row as the point to restart the general search for other holes. It then moves the file pointer down one row and determines if the pixel directly below has a value less than or equal to the threshold value. If true it then keeps moving right until it finds the right end of that row. Once the end is found, it reverses its direction and moves left, counting the pixels having "hole" values until it reaches the left end of that row. When the left end is found, the above process is repeated for the next row down except that once the left end of the third row (or odd numbered) row is found, the direction of movement is again reversed and the counting is performed moving to the right. This across-down-reverse-down-across movement is continued until no pixel in the next row is found which lies directly beneath one of the "hole" pixels in the current row. The bottom of the hole is then found, and the x and y coordinates, total number of pixels, area, perimeter and shape factors are calculated and written to an output file. The program then searches for the next hole starting at the "restart mark". When the bottom of the image is encountered, the search algorithm stops and a distribution of holes by size range is written to the output file.

Upon finding and counting each pixel within the hole and noting its location if needed, the program assigns a large value to that pixel so that the pixel would not be found later in the search for other holes. The macropore characterization algorithm was tested on known "holes" of different size and shape that were created in a small file. It successfully found and sized all holes except holes having a "U" shape, i.e. that had two separated arms. It treated such holes as two separate holes, one with an "L" shape and another as an "I" shape. An example of how the algorithm works is shown in Figure 3.4 using a threshold value of 1024. This value corresponds to $H = 0$ since 1024 is added to Hounsfield values in order to store only positive integers. The arrows show the pixel-by-pixel movement through the data up to the beginning of the third row of the hole. The shaded area shows the pixels with values less than the threshold and therefore falling within the hole.

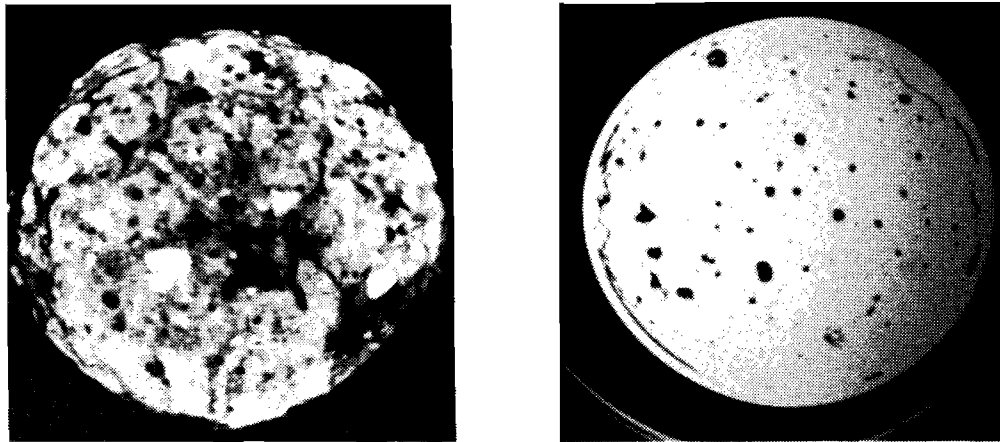
1866	1776	1633	1472	1337	1245	1265	1341	1468	1555	1653
1762	1604	1366	1131	983	897	911	1052	1256	1424	1588
1613	1338	1063	817	645	590	539	800	1020	1284	1488
1455	1088	781	571	451	440	486	652	852	1120	1377
1299	938	617	405	352	403	442	535	699	973	1273
1201	845	542	372	330	353	409	444	597	894	1250
1231	881	589	425	360	362	388	425	608	902	1299
1302	970	703	526	440	437	464	537	744	1070	1421
1442	1157	878	689	577	550	615	745	975	1258	1563
1578	1363	1096	906	811	785	818	963	1192	1451	1680
1684	1525	1345	1200	1120	1086	1137	1266	1445	1649	1785

Figure 3.4 Diagram of Step by Step Movement of Characterization Algorithm.

4. RESULTS.

4.1 Qualitative Results of Field Cores: Photos of CT Images and Physical Sections.

Photos of two CT images from the black and white CT monitor are shown in Figure 4.1. These photos were made from the images saved on photographic film at the time of the scans. Figure 4.1a is of Core 1 (grass cover, uncased) at a depth of 100 mm below the surface. The gray scale values for creation of the image are: window = 1244 and center = 891. The explanation of these parameters was given in Section 3.5. Figure 4.1b is for Core 3 (no surface cover, PVC pipe casing) at a depth of 460 mm with window = 2000 and center = -1. The photos reveal a greater variation of features in Core 1 at 100 mm than Core 3 at 420 mm, although the gray scale values do accentuate features in Figure 4.1a more than in Figure 4.1b as explained below.



a. Core 1, Depth = 100 mm

b. Core 3, Depth = 420 mm

Figure 4.1 Photos of Selected CT Images on CT Monitor.

The darkest areas in the images are the least dense while the white areas are the most dense. The smaller round dark areas are earthworm holes while the white areas are stones. The two large black areas in Figure 4.1a are ant holes. Gray areas are soil at differing densities or are roots. From these images it is clear that air-filled holes and other large density changes in the soil mass can be detected by the scanner.

The photos from the photographic film must be interpreted by eye or by means of an image analyzer. Accentuation of features by changing the gray scale cannot be done without recreating the image on the CT monitor.

Display of the scan images on a Macintosh II microcomputer was done using a black and white or gray scale as explained in Section 3. Images reconstructed using three different window and center values are shown in Figure 4.2 at a depth of 290 mm in Core 2. As with the CT monitor, black areas indicate material with a low attenuation value (low density), while white areas indicate material with a high attenuation value (high density). The image in Figure 4.2a was reconstructed using a high center value (800) and a small window (200). Consequently, there are large amounts of both black and white areas but small amounts of gray areas. The black areas could correspond to water, air or organic matter, while the white areas are either soil matrix or stones. In Figure 4.2b the center value is set at 600 and the window at 1600, resulting in black areas that are air, light areas that are soil and white areas that are small stones. In Figure 4.2c the center value is set at zero and the window at 2000, resulting in more detail of the density differences within the soil matrix but less detail for distinguishing the air-filled macropores. Part

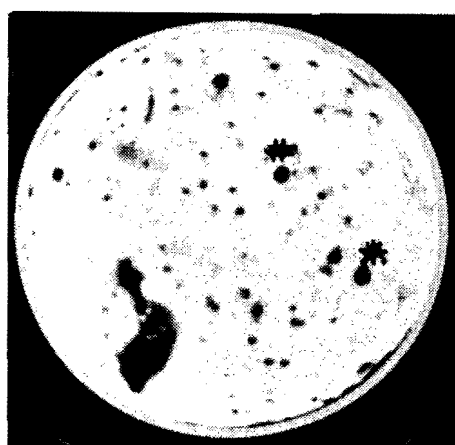
'd' of Figure 4.2 is the associated photo of the physical section taken at the time of cutting up the soil core and at the same depth as the images in Parts 'a', 'b', and 'c' of Figure 4.2.

In general the values ($C = 600$, $W = 1600$) used in generating Figure 4.2b produce the best image in comparison with features shown in the photo of the section, Figure 4.2d. The cracks in Figure 4.2d are not seen in the corresponding images and are thought to have been created during the sectioning process. The large dark area in the photo and images is an ant cavity.

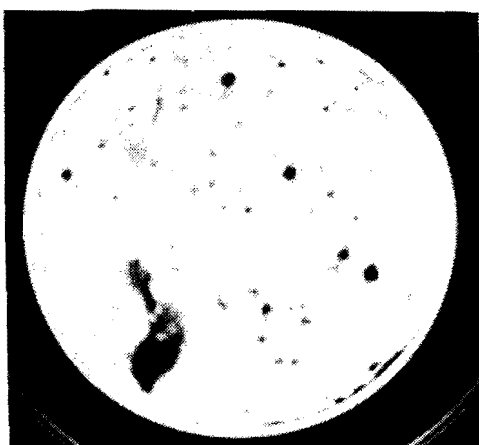
Images reconstructed on the Macintosh II are presented in Figure 4.3 for scans at other depths of Core 2. In these figures the center and window values are set as in Figure 4.2b. The gray areas in all images require further interpretation from that given above and will be discussed later. The symbols '*' and '#' on some images in Figures 4.2 and 4.3 indicate the continuous pores into which the fine sand was poured. The sand passed completely through these two large (approximately 7 mm diameter) pores, verifying their continuity from the surface to the bottom of the column (approximately 700 mm). Figure 4.4 shows displays of scans at several depths for Core 3 (Bare, PVC encased). Figure 4.5 compares a photo of the physical section and the corresponding image reconstructed on the Macintosh of some selected scans of the field cores.



a. Image with $C = 800$ and $W = 200$.



b. Image with $C = 600$ and $W = 1600$.
* and # --verified continuous pores.



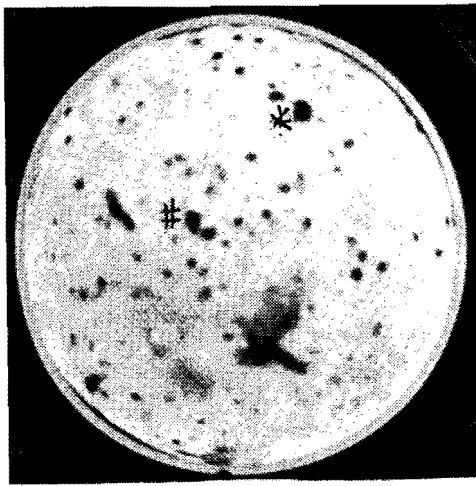
c. Image with $C = 0$ and $W = 2000$.



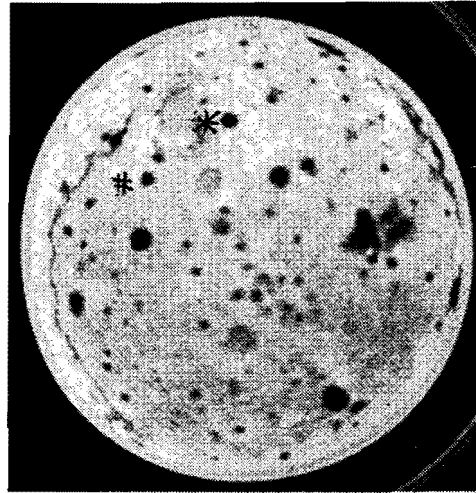
d. Photo of physical section.

Figure 4.2 Comparison of Image Settings and Physical Section for Scan at Depth = 290 mm of Core 2. [C= Center, W= Window.]

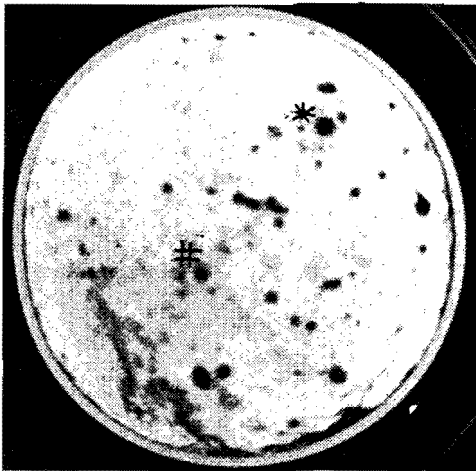
Figure 4.3 Selected CT Images on Microcomputer of Field Core 2 at Indicated Depths.
(See Fig4.XX_LongOrient100% in LONG_ORIENT folder in Thesis Clipboard folder.)



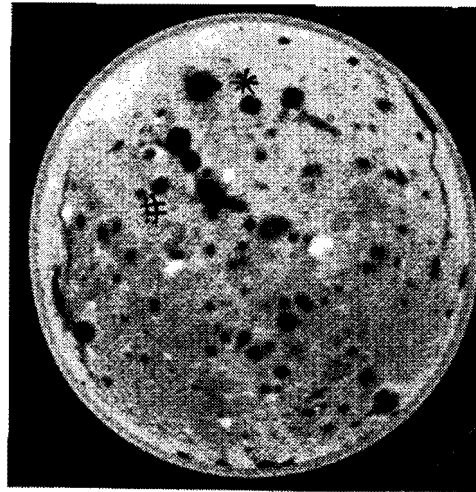
c. Depth = 250 mm.



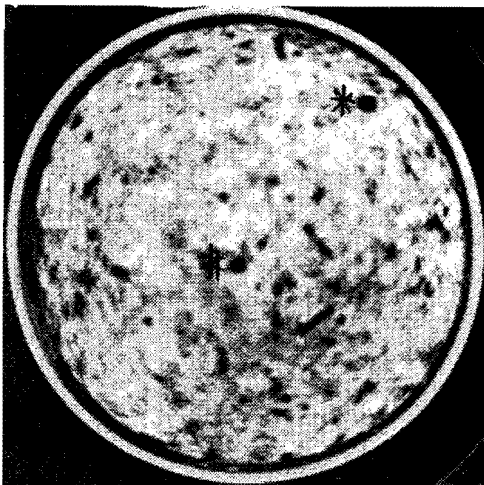
f. Depth = 510 mm.



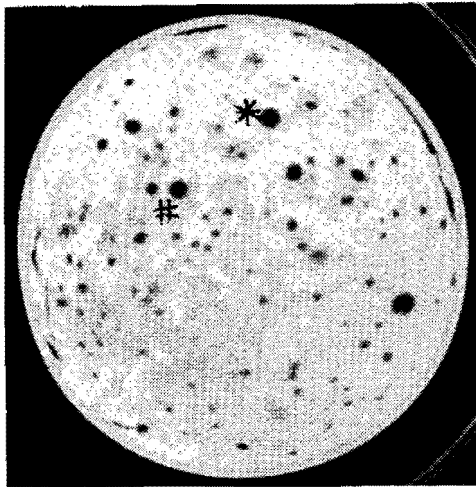
b. Depth = 170 mm.



e. Depth = 460 mm.



a. Depth = 40 mm.



d. Depth = 360 mm.

Figure 4.4 Selected CT Images on Microcomputer of Field Core 3 at Indicated Depths.
(See Fig6.XX_LongOrient100% in LONG_ORIENT folder in Thesis Clipboard folder.)

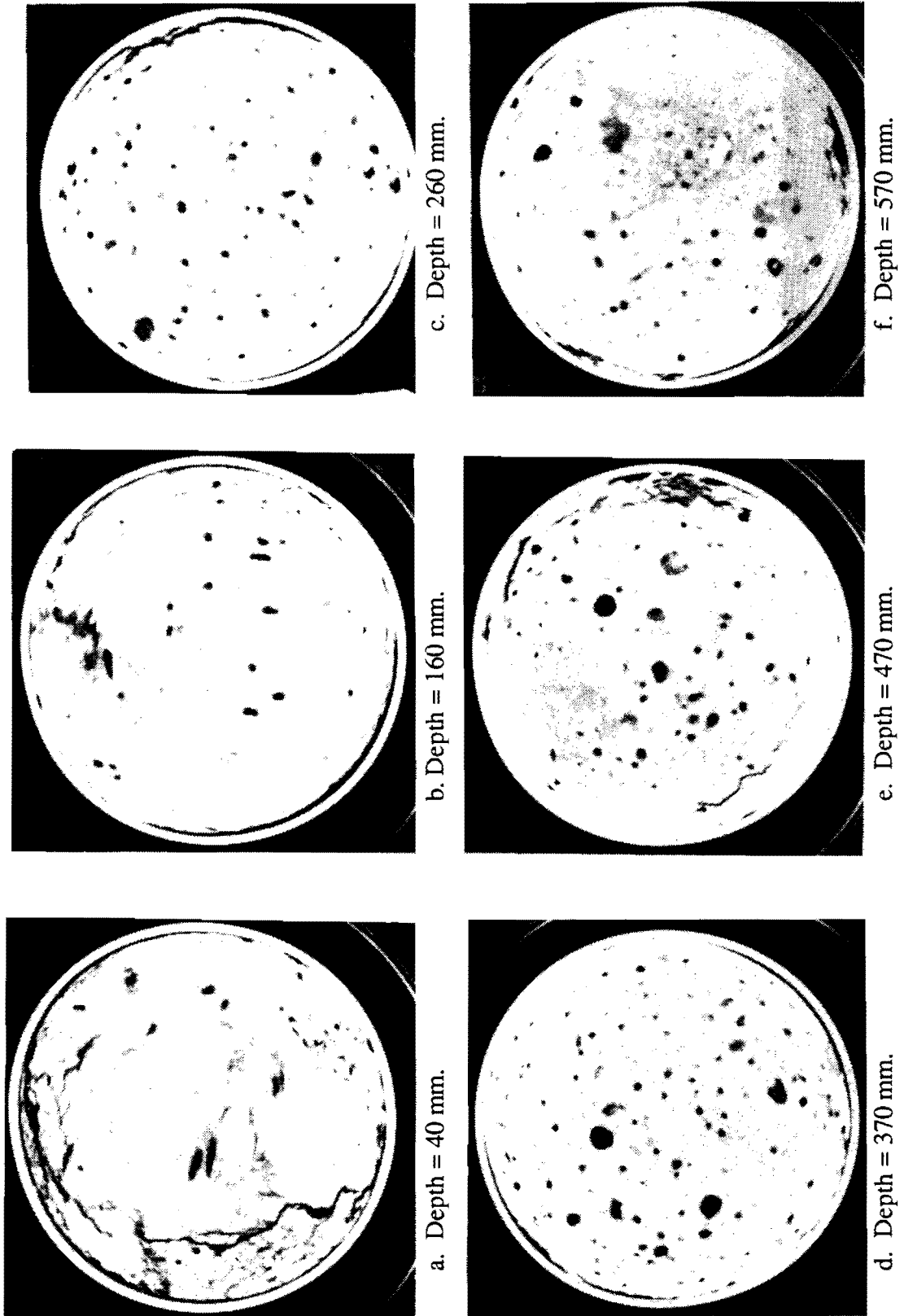
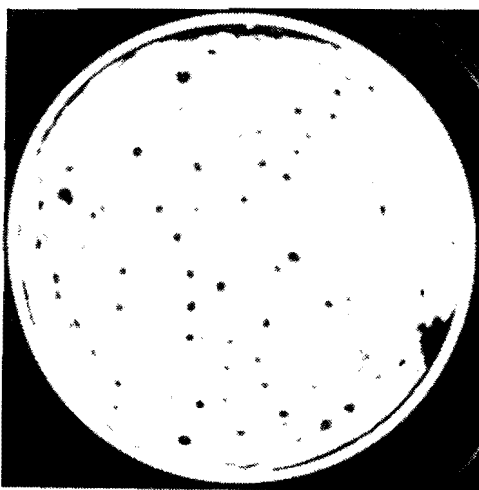
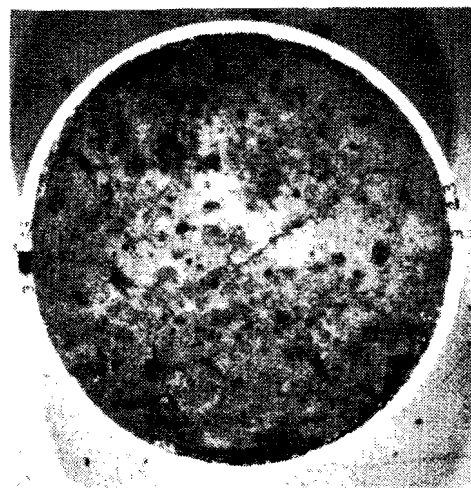


Figure 4.5 Comparison of Selected Pairs of CT Images and Physical Sections at Indicated Depths.
(See Fig6.XX_LongOrient100% in LONG_ORIENT folder in Thesis Clipboard folder.)



e. CT Image, Core 3, 280 mm



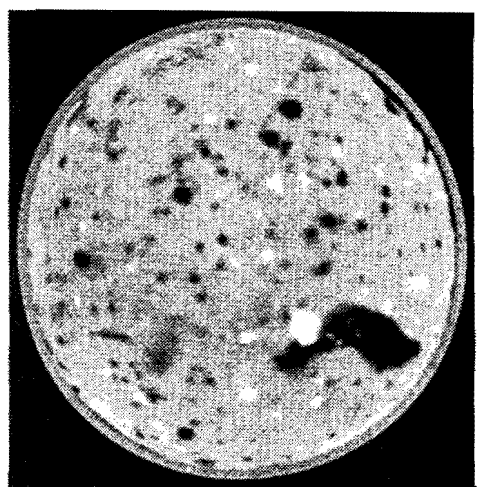
f. Section Photo, Core 3, 280 mm



c. CT Image, Core 3, 200 mm



d. Section Photo, Core 3, 200 mm



a. CT Image, Core 2, 290 mm



b. Section Photo, Core 2, 290 mm

4.2 Results of Sand and Silt Standards Analyses.

The images and data from scans of the two standards were analyzed on the Macintosh II microcomputer to accomplish some of the specific objectives mentioned at the start of Section 3. The results are reported in this section and are used in developing the appropriate values to be used in analysis of the field cores.

4.2.1 Microcomputer Images of Standards. Figure 4.6 is a black and white display recreated on the Macintosh II microcomputer of the CT image of the packed soil column with the artificially produced macropores. The image is shown in "Zoom Out" or reduced option in order to fit the page. The gray ranges of the black and white scale do not show in the figure due to the transfer into the document. Comparison of macropores shown on this image with those created in the packed soil column and shown in Figure 3.1 demonstrated that the CT scanner accurately depicted the location and size of all except the smallest macropores. The size and type of macropores in the sample are indicated in Figure 3.1.

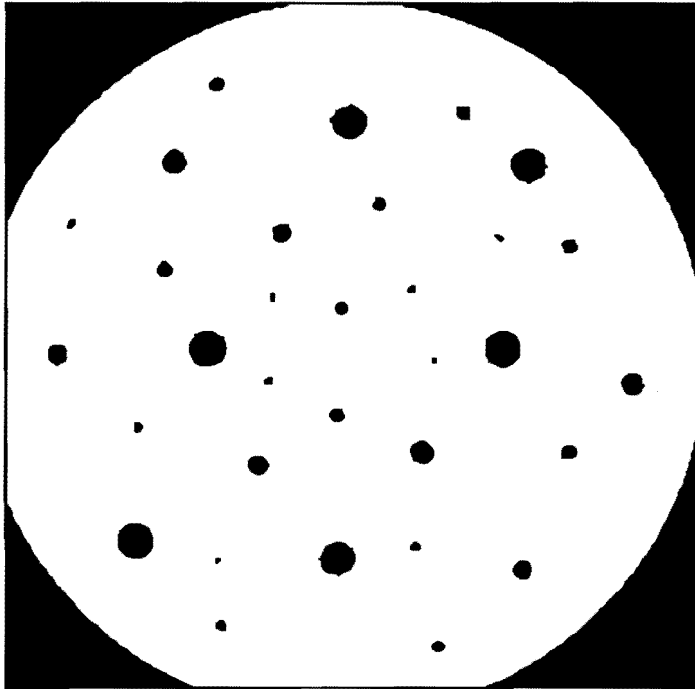


Figure 4.6 Image of Packed Column with "Macropores".

4.2.2 Accuracy of Hole Characterization. The accuracy of the CT scan method was assessed by comparing the areas of individual holes calculated by the hole characterization algorithm with the known areas of the holes in the sand and silt standards. Table 4.1 gives a summary of the areas as determined by CT for the five tubes of different

Table 4.1 Summary of Areas Determined for the Tubes in Sand Standard.

SCAN	Attenuation Threshold = 1224					Attenuation Threshold = 1124					Attenuation Threshold = 1024				
	Diameter of Tube, mm					Diameter of Tube, mm					Diameter of Tube, mm				
Slice Width (No. Scans)	0.90	1.90	2.90	4.80	7.14	0.90	1.90	2.90	4.80	7.14	0.90	1.90	2.90	4.80	7.14
Actual Hole Area, mm ²	0.64	2.84	6.60	18.10	40.08	0.64	2.84	6.60	18.10	40.08	0.64	2.84	6.60	18.10	40.08
8 mm (1) Dry Sand	0/2 <i>a</i> ----- <i>b</i> ----- <i>c</i>	1/2 2.49 -----	2/2 6.47 0.00	2/2 16.92 1.41	2/2 45.55 0.35	0/2 ----- -----	1/2 1.99 -----	2/2 5.48 0.00	2/2 16.18 0.35	2/2 43.56 1.05	0/2 ----- -----	1/2 1.99 -----	2/2 4.98 0.00	2/2 15.18 1.05	2/2 41.82 0.00
2 mm (3) Dry Sand	0/6 ----- -----	3/6 1.49 0.00	6/6 4.81 0.81	6/6 16.01 0.20	6/6 47.71 1.31	0/6 ----- -----	3/6 1.33 0.28	6/6 4.07 0.66	6/6 15.18 0.88	6/6 44.73 0.38	0/6 ----- -----	3/6 1.00 0.50	6/6 3.40 0.58	6/6 14.44 1.18	6/6 42.07 0.61
8 mm (1) Wet Sand	0/2 ----- -----	1/2 2.02 -----	2/2 5.27 0.31	2/2 16.60 0.40	1/1 <i>d</i> 47.07 -----	0/2 ----- -----	1/2 2.02 -----	2/2 4.40 0.11	2/2 15.60 0.62	1/1 <i>d</i> 45.63 -----	0/2 ----- -----	1/2 1.59 -----	2/2 4.19 0.00	2/2 14.58 0.40	2/2 <i>d</i> 42.74 -----
2 mm (4) Wet Sand	0/8 ----- -----	4/8 1.08 0.25	8/8 3.45 0.37	8/8 15.56 0.33	4/4 <i>d</i> 52.13 3.57	0/8 ----- -----	4/8 0.58 0.17	8/8 2.74 0.69	8/8 14.04 0.45	4/4 <i>d</i> 48.23 2.77	0/8 ----- -----	4/8 0.36 0.19	8/8 1.71 0.42	8/8 12.62 0.65	4/4 <i>d</i> 45.56 2.77

a Number of holes detected in scans/number of holes of size in standard

b Average area of holes detected, mm²

c Standard deviation of area of holes detected, mm²

d Only the upper plastic tube in the 8/2/89 scans is used due to water partially filling the lower tube

Table 4.2 Summary of Areas Determined for the 5 Hole Sizes in Silt Standard.
 (See S&S HoleSize file in Thesis Clipboard folder- Long Orientation at 100%).

SCAN	Attenuation Threshold = 1224					Attenuation Threshold = 1124					Attenuation Threshold = 1024				
	Hole Size Number					Hole Size Number					Hole Size Number				
Slice Width (No. Scans)	1	2	3	4	5	1	2	3	4	5	1	2	3	4	5
Actual Hole Area, mm ²	0.62	1.98	7.92	17.81	71.26	0.62	1.98	7.92	17.81	71.26	0.62	1.98	7.92	17.81	71.26
8 mm (2)	8/8 <i>a</i> 1.57 <i>b</i> 0.70 <i>c</i>	10/10 3.22 0.53	8/8 11.88 1.15	8/8 20.24 1.04	4/4 74.84 0.51	8/8 1.06 0.53	10/10 2.90 0.54	8/8 10.88 1.25	8/8 19.19 1.17	4/4 72.63 0.52	6/8 0.94 0.38	10/10 2.41 0.55	8/8 9.82 1.13	8/8 18.07 1.10	4/4 70.90 0.63
2 mm (5)	10/20 0.49 0.35	21/25 2.47 0.98	20/20 11.05 1.49	20/20 20.54 1.71	10/10 75.96 2.00	2/20 0.36 0.10	20/25 1.71 0.78	20/20 9.81 1.30	20/20 18.75 1.66	10/10 72.72 2.13	0/20 ----- -----	17/25 1.35 0.58	20/20 8.63 1.40	20/20 17.34 1.71	10/10 69.83 2.49

a Number of holes detected in scans/number of holes of size in standard

b Average area of holes detected, mm²

c Standard deviation of area of holes detected, mm²

d Only the upper plastic tube in the 8/2/89 scans is used due to water partially filling the lower tube

inside diameters in the sand standard, and Table 4.2 gives the summary for the holes formed in the silt standard by the metal rods. Only the tubes orthogonal to the x-ray beam are used in this analysis. Results for tubes at oblique angles to the x-ray beam are given in Section 4.2.4. The accuracy is dependent on the slice width of the x-ray beam, the attenuation threshold used in the algorithm for detection of a hole, on size of hole and on the density of the medium surrounding the hole. Data for individual holes can be found in Warner (1990).

For the sand standard, the 8 mm slice width gave higher area values for the glass tubes than the 2 mm slice width, but approximately equal values for the plastic tubes. There was a greater difference between the 8 mm and 2 mm values for smaller glass tubes than for larger tubes. Both 8 mm and 2 mm values underestimated the glass tube sizes for the three attenuation values (H^*) used as the threshold for hole detection, perhaps due to the dense surrounding medium of the glass which had a density of 2.22 g-cm^{-3} . H^* is equal to the Hounsfield unit (H) plus 1024, obtained in order to work with only positive integers. The H^* threshold does not have a large impact on the number of holes detected but does affect the area of the hole determined by the characterization algorithm.

The areas determined for the upper and lower plastic tubes for the 8/2/89 scans vary significantly due to the presence of some water in the lower tube. Water entered the tube through small perforations that were made in the plastic walls to perform wetting front experiments at the end of the 7/3/89 scans. The lower tube was partially full of water from those experiments. Water was unable to enter the glass tubes, but comparison of the areas for the upper and lower 4.80 mm tubes shows a consistently larger area for the lower tube. This is thought to result from the denser medium surrounding the lower tube that results from the saturated sand near the bottom of the standard.

The results indicate that there is not one value of H^* that will produce the correct area for holes of different sizes in the glass tubes. An H^* value of 1224 (equivalent to $H = +200$) still does not detect the smallest holes in the sand standard of 0.90 mm diameter even though the tube is exhibited on the image. It under predicts the area of the one 1.90 mm hole detected and does not detect the second hole of this size at 90° for either the 2 mm or 8 mm slice width. All the 2.90 mm diameter holes orthogonal to the scan beam were detected, but both slice widths underestimated the areas. The calculated area of these holes is 6.61 mm^2 . The 8 mm slice resulted in a range in area from 5.05 to 6.47 mm^2 with average value (A_{av}) for the four holes (2 holes at 90° per scan x 2 scans) of 5.87 mm^2 and standard deviation (s) of 0.72 mm^2 . The 2 mm slice area values ranged from 2.74 to 5.97 mm^2 , with $A_{av} = 4.03 \text{ mm}^2$ and $s = 0.90 \text{ mm}^2$ for 14 values. These area values are for the 7/3/89 and 8/2/89 scans. The differences in density of the medium (due to addition of water to the sand) surrounding the glass tubes appear to affect the detected area of tubes as the 8/2/89 scans had consistently lower area values than the 7/3/89 scans. This effect is examined further below.

Area values determined by the scanner for the 4.80 mm diameter hole using $H^* = 1224$ were still slightly smaller than the actual value of 18.10 mm^2 . The range was 15.93 to 17.92 mm^2 ; $A_{av} = 16.77 \text{ mm}^2$ and $s = 0.87 \text{ mm}^2$ for the 8 mm slice. For the 2 mm slice, the range was 15.16 to 16.43 mm^2 while $A_{av} = 15.75$ and $s = 0.36$.

Analysis of the areas for the 7.14 mm diameter tube (plastic) was done using only the 7/3/89 scans plus the upper tube in the 8/2/89 scans since the lower tube was partially filled with water as described above. The range was 45.31 to 47.07 mm^2 , $A_{av} = 46.06 \text{ mm}^2$ (3 values) and $s = 0.91 \text{ mm}^2$ for the 8 mm slice. For the 2mm slice, the range was 46.30 to 57.04 mm^2 , $A_{av} = 49.48 \text{ mm}^2$ and $s = 3.23 \text{ mm}^2$. The true area of the plastic tube was 40.08 mm^2 , hence both the 8 mm and 2 mm slice widths overestimated the area when the threshold of $H^* = 1224$ was used. The reason for the higher standard deviation for the 7.14 mm hole than the 2.90 mm when the 2 mm slice is used is unknown.

Average area values for the 7.14 mm hole for $H^* = 1124$ and $H^* = 1024$ are 44.25 and 42.13 mm^2 respectively for the 8 mm slice, and 46.13 and 43.46 mm^2 for the 2 mm slice. These

areas are still too large when compared to the true area but may include the plastic walls of the tube since plastic has a relatively low H value. The calculated area for the plastic tube using the outside diameter is 42.61 mm^2 .

Given the apparent influence of the medium surrounding a hole, the use of the glass or plastic tubes for determination of the threshold value is not advised. Instead the holes formed by the metal rods in the silt standard will be used since the medium surrounding the holes will closely resemble that of a natural soil containing macropores. The sand standard with the glass and plastic tubes does serve to assess the consistency of the CT scanner using multiple scans of the same object and to assess the effect of tubes at angles.

Results show that the scanner more accurately detected small holes in the silt medium than equivalent diameter glass tubes in the sand medium. Comparisons of the number detected for the 0.90 mm diameter holes in the two media show that the 8 mm slice width detected all of the holes in the silt and none in the sand. The 2 mm slice width detected 50% of the 0.90 mm holes in the silt while none was detected in the sand. Comparisons of the 1.90 mm in sand versus 1.60 mm in silt show that 50% were found in the sand while 100% and 84% were found in the silt by the 8 mm and 2 mm slice widths respectively. These comparisons are for $H^* = 1224$; but the trend of the results hold for $H^* = 1124$ and 1024 , except that the number of 0.90 mm holes detected decreases in the silt standard as H^* decreases as expected.

The area of holes measured by the scanner for the silt standard decreases with the value of H^* . All average areas for the 8 mm slice width are too large except for the 9.5 mm hole using $H^* = 1024$. The average areas for the 2 mm slice width at $H^* = 1224$ vary from being too small for 0.90 mm holes to too large for larger holes. The best overall accuracy for 2 mm is at $H^* = 1124$, but there is a small percentage of 0.90 mm holes detected. The standard deviations of areas are similar to those for the sand standard. The coefficient of variation, although not shown, is much higher for the smaller than larger holes. Again, the area of each hole for individual scans can be found in Warner (1990).

4.2.3 Surrounding Medium Effects on Attenuation Values and Hole Size. The results shown in Tables 4.1 and 4.2 reveal that the size determined by the scanner is dependent on the medium surrounding the hole. This is best shown by comparing Hole Size No. 4 in the silt standard (diameter = 4.76 mm) with the 4.80 mm diameter glass tube in the sand standard. The average area for the 4.76 mm hole in the silt standard is 20.24 mm^2 (standard deviation, $s = 1.04$, $n = 8$) while the average for the 4.80 glass tube in the sand standard is 16.92 mm^2 ($s = 1.41$, $n = 8$). These averages are for the 8 mm slice width and $H^* = 1224$. The 8 mm slice width is used for this comparison since it should give more accurate results than the 2 mm slice width for the holes orthogonal to the x-ray beam.

Another representation of the medium effects is shown in Figure 4.7 where the attenuation values for two different sized holes are graphed across the center of each hole for the mediums of different densities. The top graph of the figure shows the variation of attenuation values pixel by pixel along a horizontal centerline for the 4.76 mm (silt) and 4.80 mm (sand) holes. The silt surrounding the 4.76 mm hole has an average wet bulk density of 1.65 g cm^{-3} . The wall of the glass tube (wall thickness = 2.05 mm) has a density of 2.22 g cm^{-3} . The bottom graph of Fig. 4.9 exhibits the variation for smaller holes, specifically a 1.90 mm diameter glass tube with wall thickness of 2.85 mm versus a 1.59 mm hole in a packed silt column. The pixel dimension is 0.38 mm for all holes, and the slice width is 8 mm.

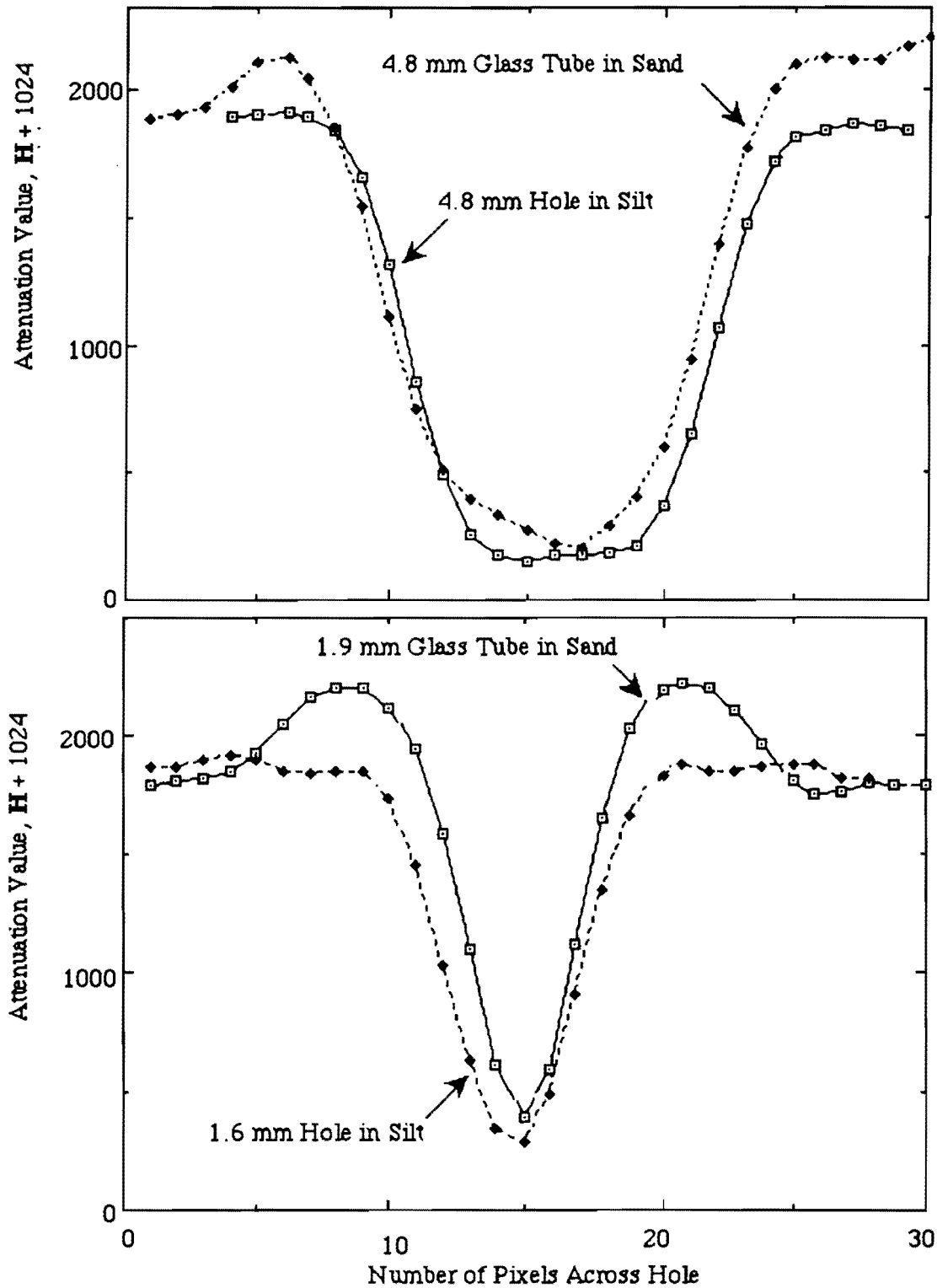


Figure 4.7 Attenuation values across holes with different medium densities.

The difference in the lowest values for the two 4.8 mm holes is small and the width of hole is only slightly smaller for the glass tube than the hole in the packed silt. However, the difference between the 1.9 mm hole in the glass tube and the 1.6 mm hole in the silt is more pronounced, both for minimum H^* and widths of the holes. The 1.6 mm hole is detected as being larger than

the 1.9 mm tube due to the relatively thick, dense wall surrounding the 1.9 mm hole. None of the minimum values for any of the holes reached the theoretical value for air of $H^* = -1000$ (equivalent to $H^* = 0$ in the graphs).

4.2.4 Comparisons of Tube Areas at Different Angles to X-ray Beam in Sand Standard.
The results for the effect of circular holes with longitudinal axis at oblique angles to the x-ray beam are given in Table 4.3. Values for 4 different sized glass tubes at two oblique angles (45^0 and 22.5^0) were compared to the 90^0 tubes for the same sizes.

Table 4.3 Areas of Tubes in Sand Standard at Different Angles to X-ray Beam.

SCAN	Tube Diam = 1.9 mm			Tube Diam = 2.9 mm			Tube Diam = 4.8 mm		
Slice Width/ Location ¹	Angle of Tube			Angle of Tube			Angle of Tube		
	90 ⁰	45 ⁰	22.5 ⁰	90 ⁰	45 ⁰	22.5 ⁰	90 ⁰	45 ⁰	22.5 ⁰
Calculated Area ²	2.84	4.01	7.41	6.61	9.34	17.26	18.09	25.59	47.29
Measured Areas in mm ² , 8/2/89 Scans, Wet Sand, Pixel Size = 0.380 mm									
8 mm TP = 0	2.02	-----	-----	5.49	3.61	-----	16.32	17.04	21.66
	-----	-----	-----	5.05	-----	-----	16.89	-----	-----
2 mm TP = 0	1.30	1.59	-----	2.74	6.79	5.34	15.16	20.50	25.56
	-----	-----	-----	3.61	-----	-----	15.60	-----	-----
2 mm TP = 10	0.87	1.88	-----	3.32	6.79	6.06	15.16	20.79	25.99
	-----	-----	-----	3.18	-----	-----	15.74	-----	-----
2 mm TP = 20	0.87	1.30	-----	3.90	6.50	6.50	15.45	20.65	25.13
	-----	-----	-----	3.61	-----	-----	16.17	-----	-----
2 mm TP = 30	1.30	1.30	0.58	3.47	6.35	6.06	15.45	20.94	26.43
	-----	-----	-----	3.75	-----	-----	15.74	-----	-----
Measured Areas in mm ² , 7/3/89 Scans, Dry Sand, Pixel Size = 0.706 mm									
8 mm TP = 0	2.49	-----	-----	6.47	3.98	-----	17.92	19.91	28.88
	-----	-----	-----	6.47	-----	-----	15.93	-----	-----
2 mm TP = 0	1.49	2.50	1.00	3.98	6.97	7.97	15.93	22.40	25.89
	-----	-----	-----	5.97	-----	-----	16.43	-----	-----
2 mm TP = 2	1.49	1.49	1.99	4.48	6.47	7.47	15.93	22.90	27.38
	-----	-----	-----	5.48	-----	-----	15.93	-----	-----
2 mm TP = 4	1.49	0.50	1.99	3.98	6.47	7.97	15.93	21.41	26.89
	-----	-----	-----	4.98	-----	-----	15.93	-----	-----

1 Location is given as relative horizontal location of Table Position (TP) in mm

2 The area for 90^0 is the area for a circle of the given diameter, while the areas for the other angles are the areas of ellipses formed by the projection of the circle onto the x-y plane for the given angle.

The hole size determined for the angles of 22.5^0 and 45^0 are larger than that for 90^0 when $H^* = 1224$ and $H^* = 1124$ but smaller when $H^* = 1024$. This results from counting more boundary pixels for higher values of H^* . With the elliptical shape resulting from the views of circular tubes at oblique angles, there is a 3-D versus only a 2-D effect for 90^0 . The perimeter-area relationships do not show a consistency for different angles.

The 7/3/89 scans and the 8/2/89 scans detected the same holes for both the 8 mm slice and 2 mm slice widths with the exception that the 1.9 mm tube at 22.5^0 was detected on only one of the 2 mm slice scans on 8/2/89 but on all 2 mm slice scans on 7/3/89. The areas determined from the 7/3/89 scans were consistently larger than the 8/2/89 scans. Both of these results may be due to the denser medium from the wet sand on 8/2/89. Both sets of scans showed that the angle of tubes had less influence on detection by the scanner than did actual size of tube or slice width. The larger

slice width fails to detect as many holes at oblique angles due to the averaging effect over 8 mm rather than 2 mm. The 8 mm slice width did give better estimates for the areas of all holes at 90⁰ than did the 2 mm slice and had less variation for holes of one size. The difference in areas for a hole as determined by the 8 mm versus 2 mm slice widths decreases as the hole size increases.

The impact of tube angle on measured area was dependent on the size of hole and on the slice width. For the 2 mm slice the measured size of hole increased with increasing angle for the 2.9 and 4.80 mm diameter holes, but showed no consistent pattern for the 1.90 mm holes. The 8 mm slice results showed a decrease in area with increasing angle for the 1.90 and 2.90 mm holes, but a small increase for the 4.80 mm holes. These results showing a difference for the 2 mm versus 8 mm slice widths are due to partial volume effects and are discussed in Section 7.3.2.

4.3 Quantitative Results for Field Cores.

4.3.1 Visual Comparison of Holes in Images with Holes in Physical Sections. Four images from Core 2 and three from Core 3 were used as representative samples for a quantitative comparison between macropores seen on the images and those marked on the physical sections. In this comparison a visual check was made to determine whether macropores found on the physical section had a corresponding macropore appearing on slides made from the film acquired directly from the CT dedicated monitor. Table 4.4 summarizes the results.

An average of 3 percent of macropores marked on the sections were not shown on the black and white CT images based on the total number shown on the images. The size of the macropores not shown was 3 mm or smaller. However, approximately 30 percent of the pores shown on the images were not marked with colored pins at the time of sectioning. Later review of section photographs revealed some apparent holes that were missed when the sections were marked. Almost all holes not marked were small, approximately 1 mm or smaller, and many were near the edge of the sections where smearing sometimes occurred during sawing of the PVC pipe.

Table 4.4 Comparison of Number of Macropores on Images with Physical Sections.

Core No./ Depth,mm	Total ¹ No. Pores On Image.	No. Pores On Image, Not on Sect.	No. Pores On Section, Not on Image.	Percent ² Missed In Section.	Percent ² Missed in Image.
2/90	36	9	4	11	25
2/130	23	4	1	4	17
2/360	45	14	0	0	31
2/510	75	24	0	0	32
3/240	45	12	2	4	27
3/370	60	23	0	0	38
3/570	26	8	0	0	31

¹ Determined from black and white images acquired directly from the CT dedicated monitor.

² Both of the percent missed on section and percent missed on the image are based on a total number of pores seen on the image (Column 2).

4.3.2 Distribution of Macropores in Core 2, Visually from Images. The visual method involved counting and sizing the macropores using the images of each scan created on the IBM-AT along with the zoom feature. This method was applied to the scans from Core 2 using color-coded images. Table 4.5 gives the size distribution of macropores for each scan. Table 4.5 also reveals the changes in total porosity of macropores with depth calculated by summing the total number of pixels with an attenuation value corresponding to that of air. The total porosity in this case is considered to represent the total volume of air in pores 1 mm or larger in diameter. The reasoning for the 1 mm threshold is explained in the Discussion section.

4.3.3 Macropore Distribution in Field Cores using Computer Characterization. The second method of determining the size distribution for scans uses the computer program written for the Macintosh II and explained in Section 4.9. This program was used to accomplish several objectives. It was used to assess the influences that the slice width and threshold value for air-filled pores made in the size determination of holes in the silt and sand standards; to determine the size variation among holes of the same size within the sand medium; to assess the ability to detect macropores at oblique angles from the scan beam; and to determine the size distribution of macropores for each scan of Cores 2 and 3, which permitted comparisons of changes in distribution with depth and tillage type. The size distributions by ranges of hole areas and total number of macropores are given for different depths in Tables 4.6 and 4.7 for Cores 2 and 3 respectively.

Table 4.5 Number of Macropores in each Image of Core 2 by Visual Determination.

Depth mm	Number of Pores ¹					Sum	Percent ² Air-filled
	< 1. mm	1.-3. mm	3.-5. mm	5.-7. mm	>7. mm		
30	21	58	26	10	5	120	3.6
40	8	43	27	9	6	93	2.0
50	6	27	23	8	3	67	1.8
60	15	28	29	5	2	79	1.7
70	6	30	27	7	3	73	3.6 ³
80	9	15	18	8	2	52	2.2 ³
90	4	14	20	5	3	46	1.1
100	2	23	19	2	2	48	3.1 ³
110	3	23	18	1	2	47	0.9
130	3	11	15	2	1	32	0.6
150	5	11	18	2	1	37	0.7
170	3	16	19	4	3	45	1.0
190	4	17	14	4	0	39	0.7
210	2	23	15	2	1	43	0.6
230	2	22	19	3	0	46	1.0
250	4	22	15	3	1	45	1.0
270	5	24	15	2	1	47	1.0
290	4	28	10	3	1	46	2.7 ³
310	10	32	14	4	1	61	0.7
360	10	40	18	5	2	75	1.1
410	10	55	36	4	2	107	1.5
460	12	32	34	3	8	89	2.6 ³
510	7	55	29	3	8	102	2.9 ³
560	4	44	13	3	4	68	3.2 ³

1. Determined from color enhanced computer displays of the images.

2. The values in this column were calculated separately, using individual pixel values.

3. These relatively large values coincided with fauna-cavity locations. See Discussion.

The numbers in Tables 4.6 and 4.7 are for an area within each image of 90749 pixels which is equivalent to 245.4 cm². The air or hole threshold value used for the numbers shown in Tables 4.6 and 4.7 was $H^* = 1224$. Lower threshold values resulted in fewer holes but showed the same trend for number of holes with depth. For Core 2 with the sod cover, the number of larger holes was fairly constant with depth while the number of small holes (and total number)

decreased rapidly within the top 50 mm for Core 2 and then gradually increased. Figure 4.8 shows the changes in the number of holes within selected ranges with depth for Core 2. The "macroporosity", defined as the volume of air-filled macropores, was calculated by dividing the number of pixels having attenuation values less than the air threshold value by the total number of pixels within the area analyzed. The changes in macroporosity with depth for different threshold values are shown in Figure 4.9.

Table 4.6 Size Distribution of Macropores with Depth in Core 2 using Computer Analysis.

Depth mm	HOLE SIZES BY RANGES, mm ² -- CORE #2							Total
	0- 1.00	1.00- 3.00	3.00- 5.00	5.00- 10.00	10.00- 20.00	20.00- 40.00	>40.00	
20	118	119	41	57	38	24	9	406
30	67	59	24	43	26	12	12	243
40	40	25	17	19	18	11	2	132
50	27	28	15	12	17	2	4	105
60	17	8	12	17	12	2	3	71
70	13	14	11	17	11	7	6	79
80	11	10	12	7	8	7	4	59
90	6	8	10	15	8	5	2	54
100	15	15	5	14	5	4	4	62
110	9	12	9	14	2	3	3	52
130	9	7	3	7	4	2	1	33
150	8	10	8	10	7	1	2	46
170	14	18	6	12	6	6	2	64
190	9	9	10	4	7	2	1	42
210	2	12	10	6	5	2	1	38
230	4	11	10	11	7	1	2	46
250	13	10	5	8	2	2	3	43
270	9	12	6	13	2	2	2	46
290	23	14	8	8	2	4	5	64
310	20	17	5	13	3	4	2	64
360	28	16	12	13	5	3	3	80
410	17	23	21	19	13	3	2	98
460	22	19	14	20	6	6	7	94
510	36	24	16	19	6	8	6	115
560	23	22	21	13	3	8	3	93

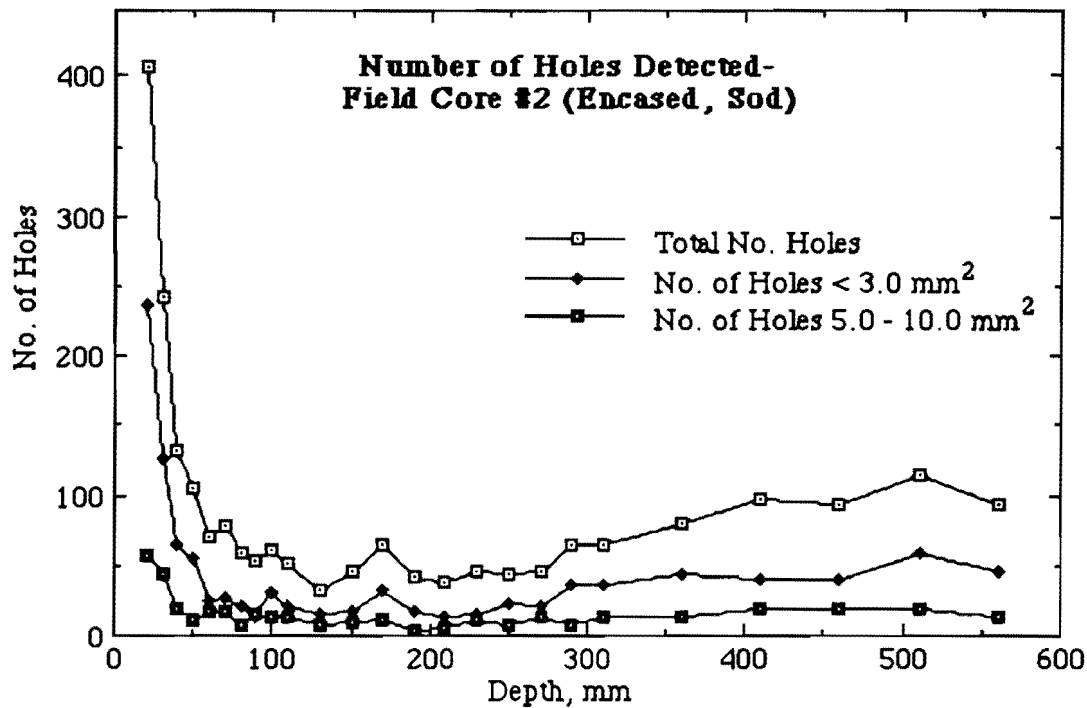


Figure 4.8 Changes in Number of Macropores with Depth for Core 2.

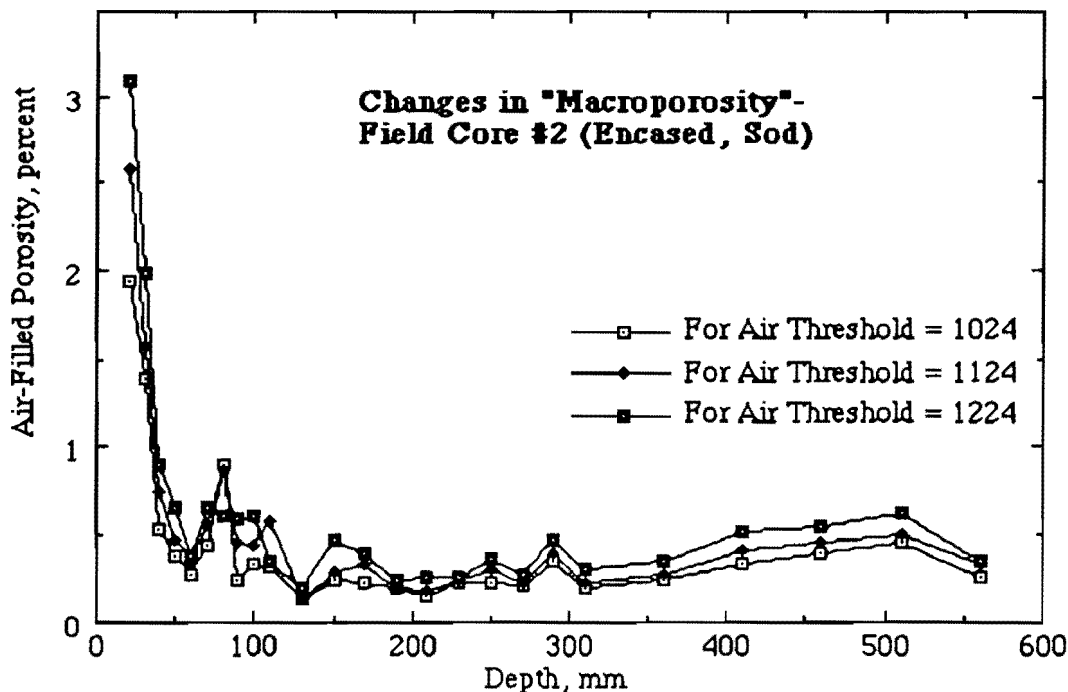


Figure 4.9 Changes in Volume of Air-filled Macropores for Core 2.

The trend in number of holes for Core 3 is similar to Core 2 except for images within the top 50 mm where the total number of holes was reduced in Core 3. The decrease was spread among the different hole sizes. The maximum number of holes occurred at a depth of 110 mm in Core 3 but at the surface in Core 2. As with Core 2, the number decreased in the mid depths of Core 3 and then increased at lower depths. However, the increase appeared to start at a lower depth in Core 3 than Core 2. The top images of Core 3 had few round "earthworm" type holes when compared to Core 2. Instead there were often larger, irregularly shaped voids or cracks near

the surface of Core 3. The changes with depth in total number of holes and number of holes within selected categories are shown in Figure 4.10, while the "macroporosity" changes are shown in Figure 4.11.

Table 4.7 Size Distribution of Macropores with Depth in Core 3 using Computer Analysis.

Depth mm	HOLE SIZES BY RANGES, mm ² -- CORE #3							Total
	0- 1.00	1.00- 3.00	3.00- 5.00	5.00- 10.00	10.00- 20.00	20.00- 40.00	>40.00	
40	46	22	10	14	7	6	4	109
50	44	27	7	13	10	8	6	115
60	38	24	8	9	14	7	6	106
70	48	27	15	13	10	9	12	134
80	51	34	13	10	16	8	7	139
90	25	27	11	7	8	5	2	85
100	49	28	15	20	10	12	4	138
110	80	59	18	24	13	13	11	218
120	25	14	10	18	6	3	2	78
140	6	7	5	4	5	2	1	30
160	5	15	5	7	7	3	0	42
180	38	33	10	21	10	5	7	124
200	22	9	10	9	9	5	2	66
220	6	10	15	8	8	2	2	51
240	5	9	8	16	5	1	1	45
260	10	17	16	15	7	2	1	68
280	12	19	13	15	5	2	1	67
300	9	24	15	11	8	1	1	69
320	10	27	15	6	7	3	3	71
370	15	36	11	16	4	3	3	88
420	23	33	11	25	6	6	3	107
470	25	25	11	11	10	3	2	87
520	10	15	9	17	3	4	0	58
570	10	5	7	10	5	2	1	40
620	28	11	7	1	6	1	2	56
670	21	11	4	6	2	0	5	49
680	12	12	6	4	7	3	1	45

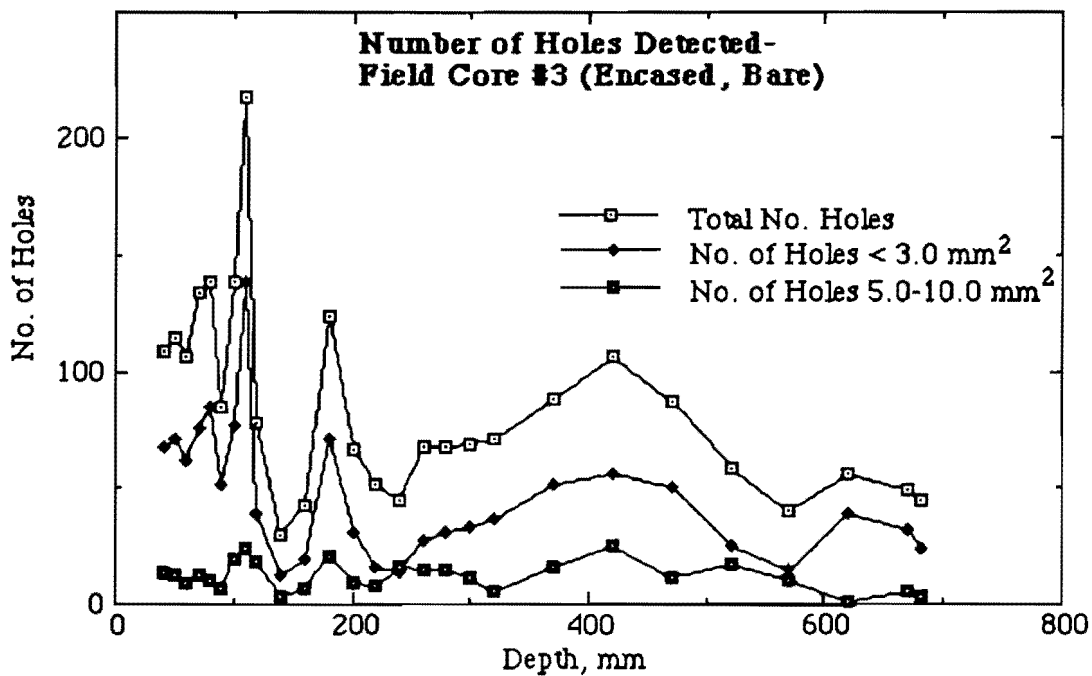


Figure 4.10 Changes in Number of Macropores with Depth for Core 3.

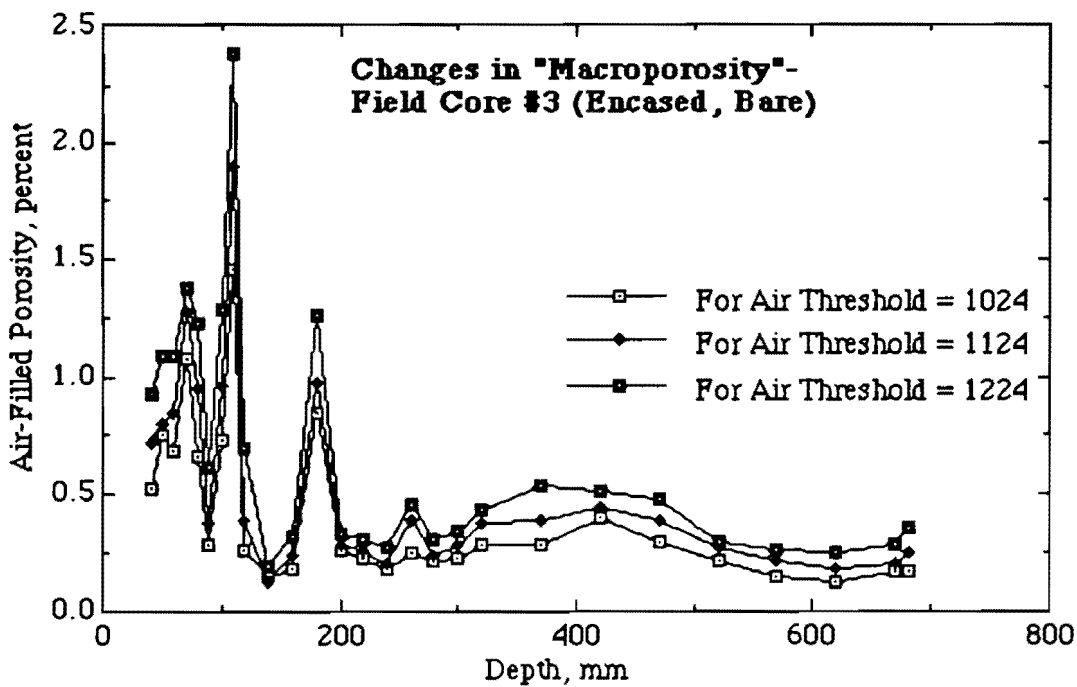


Figure 4.11 Changes in Volume of Air-filled Macropores for Core 3.

5. DISCUSSION, RECOMMENDATIONS AND CONCLUSIONS.

Discussion

5.1 Visual Identification of Macropores Using CT Images.

Macropores could be readily seen on the CT scan images reproduced on film. In general, the physical sectioning procedure verified the accuracy of the images in revealing the presence of a macropore. However, this method proved difficult in characterizing the size and distribution of macropores from image to image. The use of the color coded pins to assess the type of macropore and whether the pore was stained was helpful in assessing continuity of individual macropores from scan to scan, but was hard to assimilate into the computer characterization of the macropores.

The results shown in Table 4.1 of the comparison of the black and white scan images with the core sections showed a high correlation between the number and size of pores shown in the images with those found in the sections. At times a pore could be seen on an image that could not readily be seen on the corresponding section, but frequently probing with a pin in the section would reveal a pore that was covered by smearing or by loose soil. Very few pores were found on the sections that were not visible on the CT scan images. Any differences that occurred may have been caused by uneven section surfaces, or from a cavity formed from sectioning, or vacuuming loose material such as small stones; or may be due to boundary or partial volume effects resulting in an undetected gray area as explained above. Another possible explanation of the discrepancies is the difficulty in sectioning the core exactly at the location of the scans. If the section were made a few millimeters from the actual scan, some pores may have terminated or angled off within the small distance and show on the images but not on the section, or vice versa.

Visual identification of some macropores from the black and white images was difficult for gray-toned areas. These gray toned areas may have different origins. For example, the gray toned areas seen in Fig. 4.2a are from roots near the surface, while the large gray area near the bottom of Fig. 4.2c coincides with a cavity that had been filled with paraffin. Plugs formed from earthworm casts in old macropores in the soil may also appear gray due to a lower bulk density. Some gray areas in deeper scan images coincided with plugged earthworm channels found during the physical sectioning procedure. In addition, the gray areas could be from the boundary effect (two dimensional) or partial volume effect (three dimensional) resulting from the averaging effect of the attenuation of the x-ray beam. The pixels are actually three dimensional, being 0.536 mm by 0.536 mm by 2.0 mm long (or 8.0 mm long for the 8 mm slice width) and sometimes referred to as voxels. If a large part of the voxel is filled with air and the rest filled with a solid, the attenuation value for the voxel would be an average between that for the solid and that for the air, possibly resulting in a value corresponding to a gray shade.

5.2 Use of Microcomputers for CT Image Display and Analysis.

Use of the displays on the personal computer with either the black and white or color-coded attenuation ranges, (particularly with the enlarging "zoom" feature), provided greater ability for detailed visual examination of the scan data. The ability to change the ranges for different colors or gray scales permitted accentuation of different features such as small pores and stones on the same image. Features could be differentiated by this method. For example, pores 1.0 mm and larger in diameter could easily be distinguished when accentuated on the microcomputer. Smaller pores, down to approximately 0.5 mm, were at times distinguishable from the images but were often grayish in tone.

The use of microcomputers to exhibit and analyze the scan images also greatly enhanced the quantitative analysis of macropores in addition to the qualitative identification. A comparison of the total number of pores at corresponding depths in Tables 4.1 and 4.2 shows that the color displays (Table 4.2 data) revealed a significantly larger number of pores than the photos of scan images acquired directly from the CT dedicated monitor. Practically all of the additional pores found by the color displays were very small, 1 square mm or less in area. It was difficult to detect

these small pores by eye on the black and white CT images since the gray scale parameters were fixed. It should be noted that the ratio of the total number of pores from Table 4.1 to Table 4.2 for each depth is about the same.

Edwards et al. (1988) used a photographic/image analyzer technique to characterize macropores. After converting the numbers in Table 4.2 to a square meter basis, the total number of pores greater than 5 mm in diameter is roughly the same as the results obtained by Edwards et al. (1988). However, the total number of all pores determined in this study was much less than determined by Edwards et al. (1988). The discrepancies can be explained by the resolutions of the two methods. They were able to detect pores down to 0.4 mm in diameter, and the vast majority of the pores they found were less than 1.0 mm. They attributed pores of this size to roots and not to air-filled pores. Although some pores smaller than 1.0 mm were detected by the color-coded displays in this study, most pores shown were 1.0 mm or larger. Also, the size-range distributions given in Table 4.2 were based on the attenuation value for air-filled pores. Pixels and therefore pores having higher attenuation values corresponding to roots were not counted for this study.

Some of the voids displayed on the CT images were large, about 20 to 40 mm across. Sectioning of the cores revealed that these large voids were ant or other insect nests or burrows, some of which were filled with eggs. The ant or other fauna burrows were not evident at the surface of the core, although a few earthworm casts could be seen at the surface after removal of the grass cover. Most of these large voids were located between 70 and 200 mm below the soil surface. The numbers of pores by size shown in Table 4.2 do not include these voids as the pores were counted manually from color-coded displays on the microcomputer. However, the air-filled porosity values do include these large cavities since they were calculated by the computer. These voids were stained by the blue dye applied at the soil surface. They did not appear to be highly vertically continuous based on successive 10 mm spaced scans, but were connected by smaller holes to other voids and the soil surface as evidenced by the staining from the dye.

Each of the black and white versus color schemes for displaying images have certain advantages. The color scheme has the advantage that certain features can be accentuated for visual detection in the displays. For example, small stones or holes can be made an entirely different color than the soil mass and therefore stand out in the image when viewed by the human eye. The disadvantage of color coded ranges is that the ranges have distinct limits resulting in sharp boundaries in the image at perhaps little change in attenuation values. In other words, the image may give the impression of a large distinction for portions of an image where actually a small distinction exists. This problem can be minimized by selecting shades of the same color for the ranges. In fact this is the approach taken by assigning gray shades to the ranges in a black and white image. The black and white image therefore has the advantage of exhibiting a gradual change for small changes in attenuation value but a large change, e.g. white to black, for a large change from one pixel to another. However, the black and white images have the disadvantages of a gray scale, making contrast detection by eye difficult.

For most scanners, scan data will not vary as rapidly across pixels at abrupt edges as rapidly as the true changes in material properties due to limitations of the scanners. The sharpness of change that can be shown will depend on how the edge falls within individual pixels, the detector width, the spatial frequency of the reconstruction algorithm and other geometric factors of the system. Morgan (1983) provides an excellent explanation of these factors for CT. The color scheme can be used to show an abrupt edge more effectively than a black and white scheme.

The Macintosh and IBM each presented different programming challenges. The IBM is easier to program initially, but it is difficult to construct a program for this machine which is easy for the user. Programming for the Macintosh requires in-depth knowledge of the Macintosh interface and the built-in Macintosh user interface toolbox. But since the Macintosh is a graphics-oriented microcomputer, and since it has a well-defined standard user interface which is supported by the toolbox, the end product has the advantage of being easy to learn and use. The Macintosh toolbox also provides graphics solutions which are not available on the IBM without purchase of add-on graphics programming toolkits.

5.3 Analyses of Results from Sand and Silt Standards.

5.3.1 Accuracy of Hole Sizes Determined by Microcomputer. The results of the sand and silt standards analyses given in Section 4.2 show that the ability to accurately measure the size of macropores is dependent on several factors. Included are: the size of a macropore, the density of the medium surrounding the macropore, the attenuation threshold used for detection, the positioning of the hole with respect to the pixel coordinate system, the angle of the macropore to the x-ray beam and some scanner parameters such as the slice width and energy of the x-ray beam. The factors are not independent of each other, resulting in variations in accuracy of hole sizes for different combinations of values. As an example, the density of the medium will affect both the average and minimum values for an air-filled hole and thereby affect the size of hole measured for a given attenuation threshold as shown by Figures 4.7 through 4.9. The accuracy of measuring the sizes of holes at oblique angles to the x-ray beam is dependent not only on the angle but also on the slice width and the size of hole due to the boundary and partial effects as discussed in the next section.

The varied combinations and interactions of these factors make selection of optimal parameter values for a wide range of conditions difficult. Parameter value selection should be done for a particular objective in order to obtain the most accurate analysis for those conditions. For example, if the objective is to detect the number of very small macropores then the slice width should be made as small as possible and a high attenuation threshold should be used. However, if the objective is to accurately measure the size of medium to large sized holes that mainly lie at right angles to the x-ray beam then a larger slice width and a medium to low threshold should be used. If the objective is to assess the continuity of macropores that may meander or angle through a soil, then closely spaced scans using a small slice width should be considered. For all analyses of field cores for macropores, scans of similar materials of known density containing macropores of known sizes should be used for calibration or verification purposes using the same CT scanner.

5.3.2 Boundary and Partial Volume Effects. Although the spatial resolution as determined by the scanner and image reconstruction algorithm is approximately 0.5 mm, the practical resolution is about twice this value due to boundary effects. If the boundaries of an air-filled pore 0.5 mm in diameter exactly coincided with the pixel edges, a scan image could theoretically show that pore. However, if the pore boundary falls in the middle of the pixel, the scanner will produce an attenuation value that is an average value for the materials within the pixel, for example air and soil. The probability of a 0.5 mm pore coinciding with a 0.5 mm wide pixel is small and therefore a pore must be significantly larger than 0.5 mm to have a high probability of being detected and correctly identified. A pore 1.0 mm or larger in diameter would always completely occupy at least one 0.5 mm square pixel and theoretically should not escape detection.

The boundary effects are compounded for macropores that are not at orthogonal angles to the x-ray beam as shown by the results in Section 4.2.4. The attenuation value for a pixel is obtained for a volume (also known as a voxel) within the object. The attenuation for a voxel is therefore a function not only of the proportion of materials in the pixel cross section, i.e. boundary effects, but also any change in materials over the slice width or depth, i.e. partial volume effects.

The results in Section 4.2.4 showing a difference in measured areas of glass tubes for the 2 mm versus 8 mm slice widths are due to partial volume effects which vary with the slice. Since the attenuation value is an average value measured over the slice width, attenuation values for an 8 mm slice will have less variation than a 2 mm slice even though the means may be the same over several pixels. In other words, as the slice width increases the percentage of tube wall within the slice increases due to the oblique angle, and the minimum measured attenuation value will be higher. Therefore the 8 mm slice will detect fewer small holes at oblique angles than the 2 mm slice. The partial volume effect is more prominent for small holes than large holes. For larger diameter holes, the partial boundary effect will be less since a voxel is more likely to contain only air and not coincide with an air-wall interface along the depth of the voxel.

The spatial resolution of the scan images may depend on the diameter of the cores. The scanner used in this study had two possible fields of view, 250 mm by 250 mm resulting in 0.536 mm square pixels and 540 mm by 540 mm giving 1.0 mm square pixels. These fields of view are typical of commercially available scanners. An object larger than 250 mm would require use of the

larger field of view, resulting in a coarser resolution. The 203 mm diameter core was used to take advantage of the higher resolution of the smaller field of view. Larger cores would have the advantage of greater statistical significance for number of pores per area, but are more difficult to handle and result in loss of resolution.

The 8 mm wide slice was used for the packed columns because of the uniformity with depth of the artificial "macropores". The larger slice width has the advantage that a smoother, i.e. less "noisy", image is obtained. The slice width of 2 mm was used for the field core (the minimum possible for the scanner used) to obtain as much detail as possible. In principle the x-ray beam is spread uniformly over the slice width resulting in calculated pixel values that are an average attenuation value for the entire slice width. For uniform material with vertically straight macropores, the larger slice width would be best. However, most macropores in soil appear to meander either horizontally or vertically, and as small a slice width as possible is needed to reveal detail.

5.3.3 Beam Hardening In CT Scans. There appeared to be greater detection of very small macropores near the perimeter of the silt and sand standards than near the center. One possible explanation for this phenomenon is beam hardening as explained in Section 4.8 which results in higher average x-ray energies at the center of a scanned object than at its perimeter. Beam hardening has the effect of producing a greater attenuation value for a relatively dense object near the perimeter of a scan than for a similar object near the center of the scan. Consequently, there will be a greater contrast between the soil and a hole near the perimeter than near the center. Another explanation for the greater detection near the perimeter than center of scans could be more swelling of the silt standard at its center, but this explanation does not explain the lesser detection of small hollow glass or plastic tubes in the standards.

Figures 4.11 and 4.12, showing the change in attenuation values across a standard, indicate that some beam hardening occurred. The beam hardening will be more pronounced for the relative dense soil materials in this study than for most of the materials found in the human body. In medical applications, beam hardening is particularly noticeable in scans of the head where there is a dense material (bone) at the perimeter of the scan (Morgan, 1983). The abrupt changes in attenuation values near the perimeter of the standards could be due to changes in packing densities. However, this explanation is thought to be insignificant since care was taken to uniformly pack the standards and the beam hardening effect was seen consistently in scans of both standards and the field cores. Further evidence of the existence of beam hardening was given in Sections 4.2.5 regarding the derivation of an attenuation-density relationship where the PVC pipe surrounding the scans had a much higher attenuation value than expected for its density. These results indicate that a significant portion of the beam hardening occurred in the PVC pipe. Higher densities could have resulted near the perimeter of the field cores from the method used to obtain the cores.

The beam hardening effect for the characterization of macropores in the field cores was partially eliminated by not including the perimeter of the scans in the analysis. A diameter of 340 pixels was used for the detection and characterization of macropores in the field cores versus a total diameter of approximately 365 pixels. The analysis of only the central portions of the scans also eliminated most of the cracks and compaction effects along the walls of the container that may have resulted from core extraction, giving a more representative sample for both the macropore characterization and density determinations.

5.4 Analyses of Field Cores.

5.4.1 Macropore Distribution within Cores. Macropores were found in all field cores analyzed but varied from image to image as to the number and size. Use of the computer characterization program developed for the Macintosh II greatly facilitated the analyses of distribution of macropores in the field cores. Comparisons of the number of macropores within scans of Core 2 by visual determination and the computer characterization showed that the computer program detected more macropores especially in the top 30 mm of the core. The differences can in part be attributed to different threshold values used in the two analyses which eliminated some of the smaller macropores and shifted the number of macropores from one size range to another. Also the differences may be due to the difficulty of visually detecting very small

macropores in spite of the color differentiation used. Different size ranges were used for the computer characterization for the large sizes. The total number of macropores for the mid to lower depths was about the same for the two methods. Any differences in totals are thought to result from the non-detection of very small macropores by the visual method. The top scans were not analyzed visually due to the difficulty in counting and measuring the large number of very small macropores. Differences may also have resulted from the manner in which the computer analyzed "U" shaped holes, i.e. as an "L" shaped hole plus a "I" shaped hole.

There was not an abrupt change in the number of macropores from one image to an adjacent image with the exception of near the bottom of the tillage layer in Core 3 taken in the corn field and near the surface of Core 2 with the grass surface. The large number of macropores found in Core 2 in the top 40 mm may result from extensive earthworm and other fauna activity plus a large number of grass roots. As mentioned previously, there was a thick root mass from the grass near the surface of the core as well as evidence of the presence of earthworms, ants and other fauna. The number of holes for Cores 2 and 3 were quite similar below the tillage layer of Core 3 (about 180 mm), indicating that either earthworms were still active in the tilled area or that the holes of earthworms had persisted for long periods of time. Both cores had an increase in number of relatively large macropores (5.00 to 20.00 mm²) from a depth of about 360 to a depth of 520 mm. This increase was due to cavities that were thought to be earthworm aestivation or hibernation areas based on inspection of the physical section and on descriptions in the literature (Lee, 1985).

5.4.2 Macropore Continuity. Determination of the connectivity of individual pores using the CT scan images only, was difficult. Usually a pore was laterally displaced in comparing images at successive depths. Many appeared to be meandering vertical earthworm tunnels. Some earthworm-type pores near the edge of a core would at times be missing in successive images but would reappear farther down in the core based on visual inspection of the images and physical sections of the cores. The core may have cut off a meandering tunnel near the edge in these cases. The lateral, i.e. horizontal, meander distance was approximately 20 to 50 mm for a change in depth of 100 mm, based on 2 large macropores that could be followed from scan to scan through Field Core 2. Some of the differences in the number of pores from layer to layer shown in Tables 4.7 and 4.8 may be due to meandering, particularly for larger pores which are attributed to large earthworms such as *Lumbricus terrestris*. As reported by Lee (1985), some earthworm species form a vertical, sometimes branching tunnel. Others form predominantly horizontal tunnels that may meander randomly within certain soil layers with some openings to the surface. Still others form more or less vertical tunnels ending in roughly spherical mucous-lined chambers. Hence lateral shifts from image to image of earthworm sized macropores is not surprising. The dye stain and sectioning process indicated that some but not all connected pores were effective in water transport.

More complete assessments of the continuity and connectivity of macropores in soils using CT technology will require the reconstruction of three-dimensional images of the soil and macropore system. The methodology for reconstructing these three-dimensional images will require additional research, although a parallel methodology is already available in the medical field (Suetens et al. 1983).

Recommendations

5.5 Soil Core Collection and Analysis.

The 200 mm diameter undisturbed field core selected for the CT analysis appears to be a good size for future work, both in terms of its resolution for the scanner used and as a representative sample for the macropore distribution for the soil studied. It also provides a sample that can be manually handled. Cores of this diameter are relatively quick and easy to obtain, especially if mechanical equipment can be used for obtaining the cores. The improved techniques for soil core collection mentioned in Chapter 6, namely the use of a metal cutting edge on the bottom of the PVC pipe, the coating of the inside of the pipe with petroleum jelly and outside with

silicon, and the use of hydraulic power equipment instead of a sledge hammer for driving the pipe into the ground decreases the compaction effects on the soil near the perimeter of the core. The techniques work well for relatively wet, stone free soil but not in extremely dry or rocky soil. Techniques involving the use of mechanical digging and handling of soil cores are described by Palmer et al. (1989) and may prove necessary if cores much larger than those used in this study are needed.

The CT analysis is also relatively easy once a procedure has been developed for computer analysis of the CT data. The cost of CT scanning may be comparable or cheaper than other methods of macropore characterization when the labor needed for analyzing samples by other methods is considered. The CT scanner cost for the images obtained in this study was estimated to range from \$5.00 to \$10.00 per scan. The cost will vary with the speed at which scans can be taken. The cost above is based on a rate of \$400.00 per hour charged by a portable scanner used at small hospitals and clinics in the area. The number of scans per hour will vary with setup time and time between scans. Twenty to 30 per hour is a reasonable rate, but up to 60 per hour possibly could be done. CT analysis is applicable only when macropores greater than approximately 1mm are to be characterized if the methods and machines used in this study are representative.

5.6 Scanner Selection and Future Development.

Typical CT medical scanners have certain design features which limit their use for dense material found in geologic porous media such as soil. The ideal energy level for scanning soil materials is between 150 and 1,000 Kev in order to avoid interactions by the scatter and photoelectric effects. However, the maximum energy levels commonly available in commercial medical CT scanners of 125 to 150 Kev produce an average energy of about 70 to 80 Kev. At these energies, the Compton effect is predominate for materials common to soil, but there are other significant interactions which produce nonlinear relationships for attenuation coefficients and density. Experimental values for materials should be developed for each soil for the CT scanner being used. A standard composed of different dense materials should be scanned at the time of each experiment. This is particularly true if iron is present in a soil.

A monochromatic energy would also be much better than the polychromatic energies produced by medical scanners. Present medical scanners are adequate for qualitative detection of macropores greater than 1 mm in size, but are limited in their ability to detect smaller features and to differentiate among dense materials. Higher energy scanners would provide a better quantitative analysis of attenuation values for soil materials and therefore a better representation of density distribution within a soil sample. Higher energy scanners would also lend themselves to dual energy analysis for the differentiation of materials. Although medical scanners can be operated at different energy levels, the energies available are not suitable for distinction of materials. The relatively low energies produce too wide of response spectrum, resulting in overlapping ranges of attenuation coefficients for the energies.

Another limitation of CT medical scanners is their orientation. The x-ray source and detectors of medical scanners rotate in a vertical plane so that patients can be scanned lying down. Rotation around a horizontal plane would be best for soil analysis in order to perform dynamic flow studies under gravity.

5.7 Image Analysis.

Recommendations for further work in the image analysis include the development of software to develop a three-dimensional relationship of scan images in order to show the continuity of individual macropores and the connectivity of macropores with changes in depth. In addition to the work needed in the three-dimensional reconstruction is the need to develop further methodology to automate the interpretation of images produced. An automated system would allow the rapid determination of number, size, and character of macropores, roots, stones, and other objects present in the scan image data. The algorithms and procedures developed for image

analysis of photographs could probably be applied to such an automated system.

Another area needing further research is the edge enhancement of features in an image. For example, software is needed to better detect and define air-filled holes of different sizes. This research is especially critical since the minimum attenuation value within an air-filled hole is dependent on its size; at least this was true for the scanner used in this study. Possible approaches include searching for threshold values of pixel-to-pixel changes in attenuation coefficients (either magnitude or percentage) rather than an absolute threshold value for an air-filled hole. Changes from a moving average of pixel values could also be used.

5.8 Future Work.

In addition to the above recommendations, work should be done to investigate the use of contrast agents to temporarily fill either macropores or micropores in the soil matrix in order to provide a greater density or photoelectric effect for CT scanning. Example from the medical industry include barium and iodine which have high atomic numbers and therefore provide a contrast from surrounding low density or low atomic number materials.

The results from the hydraulic conductivity analyses indicating the hysteretic relationship between head and flow needs to be investigated further. Flow in various sized macropores, both artificial and natural, needs to be investigated using different combinations and sequences of initial and boundary conditions to determine if the non-unique head/flow relationship is a common phenomenon.

Much work in the mathematical modeling of flow in macropores is also needed in spite of much work that has already been done. Mathematical models provide the ability to assess the impacts of flow in macropores of both water and chemicals for the vast number of possibilities for combinations of different distributions of macropores, soil matrix properties, soil water contents and chemical concentrations, and application rates of water and chemicals.

Conclusions

The CT scan process is a promising nondestructive method for the characterization of macropores in soil. Pores 1.0 mm and larger in average diameter can be readily detected from the images produced from the CT scans, but the quantitative size analysis is dependent on the density and material of the surrounding medium. Although the Compton effect predominates, other photon interactions with soil materials may be significant and should be assessed for each soil material scanned. The CT process is rapid and convenient when compared to a physical sectioning process, and accurately reveals the number, size and location of macropores. Problems with obtaining smear-free, uniform-plane physical cross sections make visual identification of macropores difficult. The cost of CT scanning is reasonable compared to other methods of analysis when the labor costs are included.

The data from the CT process can be manipulated to produce images that differentiate among materials of different densities in the soil. Wet bulk densities and air-filled porosities can be calculated for cross sections at different depths in an undisturbed soil column, but the CT scanner should be calibrated by scanning standards of known materials and densities which are similar to materials to be scanned. The use of microcomputers such as an IBM-AT or PS/2 or Macintosh II greatly increases the flexibility for the display and analysis of CT scans. Customized applications for microcomputers include the display of images in color, the enhancement of certain features in the image, the selection and analysis of particular regions of interest, the graphical representation of statistics, and the visual and statistical comparisons of different images.

REFERENCES

- Anderson, J.L., and J. Bouma. 1977. Water movement through pedal soils: I. Saturated flow. *Soil Sci. Soc. Am. J.* 41: 413-418.
- Anderson, S.H., C.J. Gantzer, J.M. Boone, and R.J. Tully. 1988. Rapid Nondestructive Bulk Density and Soil-Water Content Determination by Computed Tomography. *Soil Sci. Soc. Am. J.* 52:35-40.
- Beven, K. 1981. Micro-, meso-, macroporosity and channeling flow phenomena in soils. *Soil Sci. Soc. Am. J.* 45:1245.
- Beven, K., and P. Germann. 1982. Macropores and water flow in soils. *Water Resour. Res.* 18:1311-1325.
- Beven, K., and P. Germann. 1981. Water flow in soil macropores II. A combined flow model. *J. of Soil Sci.* 32:15-29.
- Bouma, J. 1981. Comment on "Micro-, meso-, and macroporosity of soil. *Soil Sci. Soc. Am. J.* 45:1244-1245.
- Bouma, J., A. Jongerius, O. Boersma, A. Jager, and D. Schoonderbeek. 1977. The function of different types of macropores during saturated flow through four swelling soil horizons. *Soil Sci. Soc. Am. J.* 41:945-950.
- Bouma, J. and J.H.M. Wosten. 1979. Flow patterns during extended saturated flow in two, undisturbed swelling clay soils with different macrostructures. *Soil Sci. Soc. Am. J.* 43:16-22.
- Bouma, J., and L.W. Dekker. 1978. A case study of infiltration into dry clay soil. I. Morphological observations. *Geoderma* 20:27-40.
- Bouma, J., L.W. Dekker, and J.H.M. Wosten. 1978. A case study of infiltration into dry clay soil. II. Physical measurements. *Geoderma* 20:41-51.
- Brooks, R.A., and G. DiChiro. 1976. Principles of computer assisted tomography in radiographic and radioisotopic imaging. *Phys. Med. Biol.* 21:689-732.
- Brown, J.M., W.C. Fonteno, D.K. Cassel, and G.A. Johnson. 1987. Computed tomographic analyses of water distribution in three porous foam media. *Soil Sci. Soc. Am. J.* 51:1121-1125.
- Bullock, P. and A.J. Thomasson, 1979. Rothamsted studies of soil structure II. Measurement and characterization of macroporosity by image analysis and comparison with data from water retention measurements. *J. Soil Sci.* 30:391-413.
- Crestana, S., S. Mascarenhas, and R.S. Pozzi-Mucelli. 1985. Static and dynamic three-dimensional studies of water in soil using computed tomographic scanning. *Soil Sci.* 140(5): 326-332.
- Edwards, W.M., R.R. Van der Ploeg, and W. Ehlers. 1979. A numerical study of the effects of noncapillary-sized pores upon infiltration. *Soil Sci. Soc. Am. J.* 43:851-856.
- Edwards, W.M., L.D. Norton, and C.E. Redmond 1988. Characterizing macropores that affect infiltration into nontilled soil. *Soil Sci. Soc. Am. J.* 52:483-487.
- Ehlers, W. 1975. Observations on earthworm channels and infiltration on tilled and untilled loess soil. *Soil Sci.* 119(3):242-249.
- Germann, P. and K. Beven. 1981. Water flow in soil macropores I. An experimental approach. *J. of Soil Sci.* 32: 1-13.
- Germann, P.F. and K. Beven. 1985. Kinematic wave approximation to infiltration into soils with sorbing macropores. *Water Resour. Res.* 21:990-996.
- Germann, P.F., M.S. Smith, and G.W. Thomas. 1987. Kinematic wave approximation to the transport of *Escherichia coli* in the vadose zone. *Water Resour. Res.* 23:1281-1287.
- Gish, T.J. and W.A. Jury. 1982. Effect of plant roots and root channels on solute transport. Paper No. 82-2611. *Am. Soc. Agr. Engr., St. Joseph, MI.*
- Green, R.D. and G.P. Askew. 1965. Observations on the biological development of macropores in soils of Romney Marsh. *J. Soil Sci.* 16(2):342-349.
- Hainsworth, J.M., and L.A.G. Aylmore. 1983. The use of computer-assisted tomography to determine spatial distribution of soil water content. *Aust. J. Soil Res.* 21:435-443.

- Hainsworth, J.M., and L.A.G. Aylmore. 1986. Water extraction by single plant roots. *Soil Sci. Soc. Am. J.* 50:841-848.
- Harr, R.D. 1977. Water flux in soil and subsoil on a steep forested slope, *J. Hydrol.* 33:37-58.
- Hewlett, J.D. and A.R. Hibbert. 1967. Factors affecting the response of small watersheds to precipitation in humid areas. In: W.E. Sopper and H.W. Lull (eds.), *Forest Hydrology*. Pergamon Press.
- Hubbell, J.H. 1969. Photon cross sections, attenuation coefficients, and energy absorption coefficients from 10 keV to 100 GeV. U.S. Department of Commerce. National Bureau of Standards. Washington, D.C.
- Jongierius, A., D. Schoonderbeek, A. Jager, and S.T. Kowalinski. 1972. Electro-optical soil porosity investigation by means of a Quantimet B equipment. *Geoderma* 7:177-198.
- Klaseus, T.G., G.C. Buzicky, and E.C. Schneider. 1988. Pesticides and groundwater: Surveys of selected Minnesota wells. Minn. Dept. of Health and Minn. Dept. of Agric., St. Paul, MN.
- Lee, K.E. 1985. Earthworms: Their Ecology and Relationships with Soils and Land Use. Academic Press, Sydney, Australia.
- Luxmoore, R.J. 1981. Micro-, meso-, and macroporosity of soil. *Soil Sci. Soc. Am. J.* 45:671-672.
- McCullough, E.C., 1975. Photon attenuation in computed tomography. *Med. Phys.* 2:307-320.
- Moore, I.D., G.J. Burch, and P.J. Wallbrink. 1986. Preferential flow and hydraulic conductivity of forest soils. *Soil Sci. Soc. Am. J.* 50:876-881.
- Morgan, C.L., 1983. Basic Principles of Computed Tomography. University Park Press. Baltimore, Maryland.
- Mosley, M.P. 1979. Streamflow generation in a forested watershed, New Zealand. *Water Resour. Res.*, 15(4):795-806.
- Mosley, M.P. 1982. Subsurface flow velocities through selected forest soils, South Island, New Zealand. *J. Hydrol.* 55:65-92.
- Office of Technology Assessment. 1984. Protecting the nation's groundwater from contamination. OTA-O-233, Vol. 1. Congress of the United States. Washington, D.C.
- Omoti, U. and A. Wild. 1979. Use of fluorescent dyes to mark the pathways of solute movement through soils under leaching conditions: 2. Field experiments. *Soil Sci.* 128(2):98-104.
- Palmer, R.E., J.J. Messinger, and W.L. Magette. 1989. Collection and air permeability evaluation of undisturbed lysimeters. Paper No. 89-2548. *Am. Soc. Agr. Engr.*, St. Joseph, MI.
- Parsons, D.W. and J.M. Witt. 1988. Pesticides in groundwater in the United States of America. A report of a 1988 survey of state lead agencies. Department of Agricultural Chemistry, Oregon State Univ., Corvallis, Oregon.
- Petrovic, A.M., J.E. Siebert, and P.E. Rieke. 1982. Soil bulk density analysis in three dimensions by computed tomographic scanning. *Soil Sci. Soc. Am. J.* 46:445-450.
- Pikul, J.K., Jr., J.F. Zuzel, and D.E. Wilkins. 1988. Measurement of tillage induced soil macroporosity. Paper No. 88-1641. *Am. Soc. Agr. Engr.*, St. Joseph, MI.
- Rahe, T.M., C. Hagedorn, E.L. McCoy, and G.F. Kling. 1978. Transport of antibiotic-resistant *Escherichia coli* through Western Oregon hillslope soils under conditions of saturated flow. *J. Environ. Qual.* 7(4):487-494.
- Richard, T.L., N.B. Pickering, J.-Y. Parlange, and W.J. Waltman. 1988. Macropore influences on chemical movement in soil. Paper No. NAR-88-401. *Am. Soc. Agr. Engr.*, St. Joseph, MI.
- Richard, T.L., and T.S. Steenhuis. 1987. Tile drain sampling of preferential flow on a field scale. *Trans. Am. Geophys. Union* 68(16):314.
- Ringrose-Voase, A.J., and P. Bullock. 1984. The automatic recognition and measurement of soil pore types by image analysis and computer programs. *J. of Soil Sci.* 35:673-684.
- Smettem, K.R.J., and N. Collis-George. 1985a. Statistical characterization of soil biopores using a soil peel method. *Geoderma* 36: 27-36.

- Smettem, K.R.J., and N. Collis-George. 1985b. The influence of cylindrical macropores on steady-state infiltration in a soil under pasture. *J. of Hydrology* 79(1985):105-114.
- Smettem, K.R.J., and N. Collis-George. 1985c. Prediction of steady-state ponded infiltration distributions in a soil with vertical macropores. *J. of Hydrology* 79(1985):115-122.
- Steenhuis, T.S., M.S. Andreini, and J.Y. Parlange. 1988. A numerical model for preferential solute movement. Paper No. 88-2631. Am. Soc. Agr. Engr., St. Joseph, MI.
- Steenhuis, T.S., T.L. Richard, M.B. Parlange, S.O. Aburime, and J.Y. Parlange. 1986. Preferential flow influences on drainage of shallow sloping soils. Paper No. 86-2551. Am. Soc. Agr. Engr., St. Joseph, MI.
- Stillwater, R. and A. Klute. 1988. Improved methodology for a collinear dual-energy gamma radiation system. *Water Resour. Res.* 24:1411-1422.
- Suetens, P., P. Jansen, A. Haegemans, A. Oosterlinck, and J. Gybels. 1983. 3D reconstruction of the blood vessels of the brain from a stereo pair of subtraction angiograms. *Image and Vision Computing* Vol. 1(1): 43-51.
- Thomas, G.W., and R.E. Phillips. 1979. Consequences of water movement in macropores. *J. Environ. Qual.* 8(2):149-152.
- Tollner, E.W., J.W. Cheshire, Jr., and B.P. Verma. 1987. X-ray computed tomography and nuclear magnetic resonance for studying soil systems. *Proc. Int. Conf. on Measurement of Soil and Plant Water Status: Vol. 1*, Utah State University, Logan, UT. p. 247-253.
- Tollner, E.W., and L.E. Ramseur. 1988. Using computed tomography to measure soil moisture and bulk density in the presence of a growing plant. Paper No. 88-1625. Am. Soc. Agr. Engr., St. Joseph, MI.
- Tollner, E.W., and B.P. Verma. 1987. X-ray CT for soil moisture analysis. Paper No. 87-1555. Am. Soc. Agr. Engr., St. Joseph, MI.
- U.S.G.S. 1989. Reconnaissance sampling finds herbicides in streams in 10 midwestern states. News release of Nov. 15, 1989 Public Affairs Office, U.S. Geological Survey, Reston, Virginia.
- Wang, S. Y-D. 1983. Computer assisted tomography and its application in the study of multiphase flow through porous media. Ph.D. Thesis. Columbia Univ. New York, N.Y.
- Warner, G.S. 1990. Characterization of soil macropores by computed tomography. Ph.D. Thesis. Univ. of Minnesota. St. Paul, MN.
- Warner, G.S. and D.J. Hansen. 1989. Microcomputer display of CT and MRI data. Paper No. 89-7524. Am. Soc. Agr. Engr., St. Joseph, MI.
- Watson, K.W., and R.J. Luxmoore. 1986. Estimating macroporosity in a forested watershed by use of a tension infiltrometer. *Soil Sci. Soc. Am. J.* 50: 578-582.
- Whipkey, R.Z. 1967. Theory and mechanics of subsurface stormflow. p.255-260. *In* W.E. Sopper and H.W. Lull (ed) *Int. Symp. of For. Hydrol., Natl. Sci. Found., 29 Aug- 10 Sept. 1965, Pennsylvania State Univ., University Park, Pa.* Pergmon Press, New York.
- White, D.R. 1978. Tissue substitutes in experimental radiation physics. *Med. Phys.* 5(6):467-478.
- Wild, A., and I.A. Babiker. 1976. The asymmetric leaching pattern of nitrate and chloride in a loamy sand under field conditions. *J. Soil Sci.* 27:460-466.